MŰEGYETEM 1782

Budapest University of Technology and Economics
Department of Applied Mechanics

Szabolcs Berezvai

Experimental and numerical investigation of the effects of surface skin layer on the overall behavior of polymer foams

BSc Thesis

Supervisor: Dr. Attila Kossa, Assistant Professor

Budapest, 2013

MŰEGYETEM 1782

SZAKDOLGOZAT FELADAT (BSc)

A feladat címe: **Felületi bőrrétegnek az eredő anyagi viselkedésre gyakorolt hatásának kísérleti és numerikus vizsgálata polimer hab alapanyag esetén**

A szakdolgozat készítője (kódja): **Berezvai Szabolcs (C22N59)**

Alapszak / szakirány: Mechatronikai mérnöki alapszak / Gépészeti modellezés szakirány

Tanszéki konzulens neve,beosztása: Dr. Kossa Attila, adjunktus
munkahely neve, címe: Műszaki Mechanikai Tanszék
1111 Budapest, Műegyetem rkp. 5.

Külső konzulens neve, beosztása: ---
munkahely neve, címe: ---

A feladat részletezése:

1. Röviden ismertesse a polimer habok cellastruktúráit, valamint a mechanikai terhelés hatására fellépő jellegzetes deformációs jelenségeket.
2. Foglalja össze a makroszerkezeti viselkedés modellezésére alkalmas hiperelasztikus anyagmodelleket.
3. Javasoljon módszert a felületi bőrréteg eltávolítására és készítsen elő próbatesteket a mérésekhez.
4. Végezzen húzó- és nyomóméréseket az elkészített alapanyagokon és értékelje ki a méréssel kapott eredményeket.
5. Illessze a méréssel kapott adatokhoz a kiválasztott hiperelasztikus anyagmodell paramétereit, valamint készítsen végeselemes analíziseket a felületi bőrréteg hatásának vizsgálatára.
6. Foglalja össze az eredményeit magyar és angol nyelven.

Feladat kiadása / beadási határidő: **2013. szeptember 9. / 2013. december 13.**

Záróvizsga tárgyak (kód):

1. Mechatronika (BMEGEFOAMM1, BMEGEFOAMM2)
2. Analóg és digitális technika (BMEVIAUA009, BMEVIAUA010)
3. Robotok mechanikája és áramlások numerikus modellezése (BMEGEMMAM32, BMEGEÁTAM04)

Budapest, 2013. szeptember 9.

……………………………………………
tanszékvezető

A feladatot jóváhagyom:

Budapest, 2013. szeptember 9.

……………………………………………
dékán

Alulírott a feladatkiírás átvételével egyúttal nyilatkozom, hogy a szakdolgozat előkövetelményeit maradéktalanul teljesítettem. Ellenkező esetben tudomásul veszem, hogy a jelen feladatkiírás érvényét veszti.
Budapest, 2013. szeptember 9.

……………………………………………
hallgató

Contents

1 Introduction **1**
- 1.1 Aim of the work . . . 1
- 1.2 Outline of the thesis . . . 2
- 1.3 Nomenclature . . . 3

2 Mechanical behaviour of elastomeric polymer foams **5**
- 2.1 Introduction . . . 5
- 2.2 Mechanical properties in compression . . . 6
  - 2.2.1 Linear elasticity . . . 6
  - 2.2.2 Non-linear elasticity and densification . . . 9
- 2.3 Mechanical properties in tension . . . 10

3 Measurements **11**
- 3.1 Introduction . . . 11
- 3.2 Compression tests . . . 14
  - 3.2.1 Description of the test, geometry of specimens . . . 14
  - 3.2.2 Machine direction . . . 18
  - 3.2.3 Non-machine direction . . . 20
  - 3.2.4 Thickness . . . 22
  - 3.2.5 Summary . . . 24
- 3.3 Tensile tests . . . 24
  - 3.3.1 Description of the test, geometry of specimens . . . 24
  - 3.3.2 Machine direction . . . 27
  - 3.3.3 Non-machine direction . . . 29
  - 3.3.4 Summary . . . 31
- 3.4 Results of measurements . . . 31

4 Hyperelastic model fitting **33**
- 4.1 Introduction, theoretical summary . . . 33
- 4.2 Ogden–Storåkers compressible hyperelastic model . . . 34
  - 4.2.1 Description of the model . . . 34
  - 4.2.2 Solutions for homogenous deformations . . . 35
- 4.3 Determination of material parameters . . . 36
  - 4.3.1 Introduction . . . 36
  - 4.3.2 Relation of stretches . . . 37
  - 4.3.3 Correction factor . . . 38
  - 4.3.4 Procedure of fitting . . . 39
  - 4.3.5 Results . . . 40
    - 4.3.5.1 Compression - Machine direction . . . 40
    - 4.3.5.2 Compression - Non-machine direction . . . 42

4.3.5.3 Compression - Thickness . . . 43
4.3.5.4 Tension - Machine direction . . . 45
4.3.5.5 Tension - Non-machine direction . . . 46
4.3.6 Summary . . . 48

5 Finite element analysis 49
5.1 Introduction . . . 49
5.2 Simulation of the experiments . . . 50
5.3 Results of simulations . . . 51
5.3.1 Compression - Machine direction . . . 51
5.3.2 Compression - Non-machine direction . . . 52
5.3.3 Compression - Thickness . . . 52
5.3.4 Tension - Machine direction . . . 53
5.3.5 Tension - Non-machine direction . . . 54
5.4 Evaluation of simulation . . . 55

6 Summary of results 57
6.1 Summary in English . . . 57
6.2 Summary in Hungarian (Az eredmények összefoglalása) . . . 59

References 62

Appendix 63

Nyilatkozat

Alulírott Berezvai Szabolcs kijelentem, hogy ezt a dolgozatot meg nem engedett segédeszköz nélkül, saját magam készítettem, és abban csak a megadott forrásokat használtam fel. Minden olyan részt, amelyet szó szerint idéztem, vagy azonos tartalomban, de átfogalmazva más forrásból átvettem, egyértelműen, a forrás megadásával jelöltem.

Budapest, 2013. december 13.

Berezvai Szabolcs

Acknowledgements

First of all, I would like to thank my Supervisor, Dr. Attila Kossa (Department of Applied Mechanics) for his outstanding guidance and constant support during my work. I also thank János Szücs, laboratory engineer (Department of Machine and Product Design) the laser-cut specimens for tensile test.

This research has been supported by the Hungarian Scientific Research Fund, Hungary (under Contract: OTKA, PD 108691). This support is gratefully acknowledged.

Finally, I am also thankful for my Mum, who inspired me to be an engineer, my family and my Girlfriend, Viki for their patience and unwavering support during my whole BSc program.

1 Introduction

1.1 Aim of the work

Nowadays, polymer foams are widely applied cellular materials in the field of industry, used primary in packaging. In this application, the polymer foam should absorb all kinetic energy of the impact, protecting the product inside. The applications require the complete understanding of the mechanical behaviour of the foam, which is affected by the so-called surface skin layer. [10] [15] [20]

The skin layer is a thick layer on the surface of the polymer foam created unwittingly during the manufacturing. In this layer the material properties change, become inhomogeneous therefore it affects the mechanical behaviour of the foam.

The goal of the thesis is to investigate this effect by experimental and numerical methods, in order to understand the material behaviour of polymer foams. Firstly a series of tensile and compression test will be executed on specimens of a specific polyethylene foam, in order to determine the difference of mechanical behaviour between specimens containing and non-containing the skin layer.

After, a proper hyperelastic model (Ogden–Storåkers compressible hyperelastic model) will be fitted to the stress-stretch characteristics. Having found the coefficiens based on the measurement data of our polyethylene foam, we will receive an adequate material model for numerical methods.

Additionally, the measurements will be simulated by finite element analysis in order to compare the results received by the tests and by applying the fitted material model.

1.2 Outline of the thesis

The structure of the BSc thesis based on the aims of the work contains 6 chapters, including the chapter of introduction (*Chapter 1*), where the goals, the structure and the applied notations are presented.

In *Chapter 2*, the summary of the mechanical behaviour of polymer foams can be found. This chapter is based on the following piece of scientific literature: Lorna J. Gibson and Michael F. Ashby: Cellular solids: structure and properties (1997) [10]. The summary represents the basic structures of polymer foams used for describing the characteristic of deformation in case of compression and tension. The material properties, required for determine the exact mechanical behaviour, are also provided in case of all structure types.

After, in *Chapter 3*, the measurements executed on our specific polyethylene foam are presented, which goal is to investigate the effect of the skin layer. Compression and tensile tests were executed on 4-4 specimens per each direction with and without layer based on the proper International (ISO)[7] and the American (ASTM) standards [9], [8]. The geometry of specimens, the parameters of test, the evaluation and the results are also represented in this chapter, which shows the effect of skin layer by measurements.

Chapter 4 provides the theory of hyperelasticity based on the literature of continuum thesis Issam Dorghi: Mechanics of Deformable Solids (2000) [5]; Allan F. Bower: Applied mechanics of solids (2010) [3] and EA. de Souza Neto *et al.*: Computational methods for plasticity: theory and application (2008)[4]. Firstly the theoretical summary of hyperelastic models and the most commonly used model for compressible foams, the Ogden–Storåkers model are presented [11] . The aim of this chapter is to fit this material model to our measured and video-processed data, thus creating the hyperelastic description of the mechanical behaviour in all directions.

In *Chapter 5*, the fitted hyperelastic model is applied in finite element analysis (in *ANSYS*) in order to investigate numerically the behaviour of the fitted material model and to compare it with the measured data.

In the end, in *Chapter 6*, the summary of the results and the conclusion are peresented in English and Hungarian as well.

The thesis also contains an *Appendix* in which the *Wolfram Mathematica* [18] notebooks, used for post-processing the measurement data, are presented.

1.3 Nomenclature

Latin letters

A_0	Area of the initial cross-section
$\boldsymbol{b}$	Left Cauchy-Green deformation tensor
b	Initial thickness of specimens
$\boldsymbol{C}$	Right Cauchy-Green deformation tensor
C	Numeric constant
c	Correction factor
e	Error of model fitting
E	Elastic (Young's) modulus
$\boldsymbol{F}$	Deformation gradient
F	Load
G	Shear modulus
H_0	Initial separation of the Test System
I	Second moment area with respect to the axis of bending
I_1, I_2, I_3	Principal invariants of $\boldsymbol{C}$ and $\boldsymbol{b}$
J	Volume ratio (determinant of $\boldsymbol{F}$)
l	Representative length of polymer cell
L_0	Inital compression or tension length of specimens
$\boldsymbol{n}^{(a)}$	Unit eigenvectors of the left Cauchy-Green deformation tensor
p	Pressure
P	1st Piola-Kirchhoff stress (engineering stress or nominal stress in 1D)
$\boldsymbol{P}$	1st Piola-Kirchhoff stress tensor
t	Wide of the cell edge
v	Speed of crosshead
V	Representative volume of cell
w	Width of specimens
W	Elastic potential measured per unit reference volume

Greek letters

α_i, β_i, μ_i	Material parameters of the Ogden–Storåkers model
γ	Shear-strain
δ	Linear-elastic deflection
ε	Engineering strain
$\dot{\varepsilon}$	Engineering strain rate
λ	Stretch
ν	Poisson's ratio
ρ	Density
σ	Cauchy-stress in 1D
$\boldsymbol{\sigma}$	Cauchy stress tensor
τ	Shear stress
τ_A	Principal Kirchhoff stress ($A = 1, 2, 3$)
$\boldsymbol{\tau}$	Kirchhoff stress tensor
ψ	Elastic potencial measured per unit mass

2

Mechanical behaviour of elastomeric polymer foams

The following theoretical summary is based on the book, titled *Cellular solids: Structure and properties* by Lorna J. Gibson & Michael F. Ashby, Cambridge University Press, 1997 [10].

2.1 Introduction

The usage of polymer foams can strongly depend on its mechanical behaviour, even when the primary use is not mechanical. Therefore understanding the mechanics of foams is highly required. Mechanical properties of a foam are related to its structure (*open* or *closed*) and the following material properties of the cell: relative density (ρ^*/ρ_s), density of the cellular material (ρ_s), Young's modulus of the cellular material (E_s) and the yield strength (σ_s).

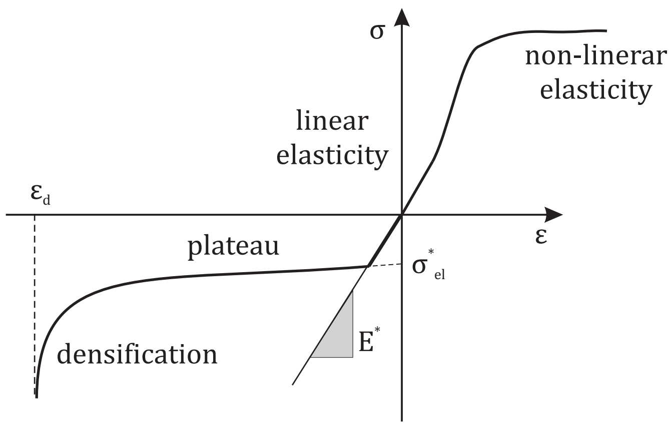

Figure 2.1: Stress-strain curve of elastomeric polymer foams

The deformation mechanisms in an elastomeric polymer foam can be analysed by the stress-strain curve, which is shown in Figure 2.1. The deformation can be divided into two parts: compression and tension. In case of compression the curve shows *linear elasticity* at low stresses, this is followed by a long *collapse plateau* and finally by the regime of *densification*. The linear elasticity is caused by *cell-wall bending*, plus *cell-face stretching* if the cells are closed. The plateau is associated with the collapse of cells, in case of elastomeric foams it means *elastic buckling*. At the densification, due to the collapse, cell walls touch each other and the cellular solid itself starts to compress. When the loading is tensile, similarly to the compression part at low stresses linear elasticity can be observed, after it the stress-strain curve becomes non-linear due to the increasing stiffness caused by the rotation of cell edges towards the tensile axis, while it fractures.

2.2 Mechanical properties in compression

2.2.1 Linear elasticity

The linear behaviour of an elastomeric foam can be described by a couple of moduli. In case of isotropic foams two moduli are required, which are chosen from: the Young's modulus (E^*), the shear modulus (G^*) and the Poisson's ratio (ν^*). In order to give the proper expressions for the moduli in demand, the structure of the cells should be determined, because the mechanism depends on whether they are open or closed. In case of open-cells, besides the cell-wall bending, deformation mechanism can be described by the axial deformation of cell-walls and the fluid flow between the cells. Although, when cells are closed cell-wall bending, edge contraction, membrane stretching and the pressure of the enclosed gas contributes the linear elastic response. These mechanisms are presented in Figure 2.2.

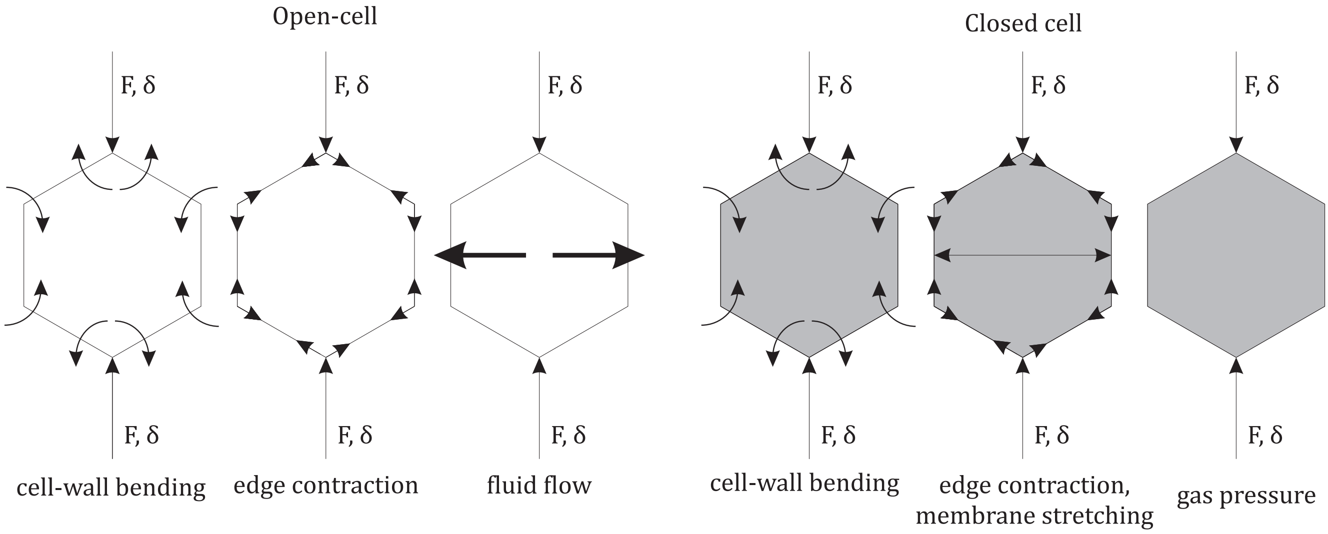

Figure 2.2: The mechanisms of deformation

Open cells

An open-cell foam can be modelled as a cubic array of members with a length (l) and a square cross-section of side (t). The relative density of the cell (ρ^*/ρ_s) and the second moment area of a member (I) are related to the following geometrical dimensions:

$$\frac{\rho^*}{\rho_s} \approx \left(\frac{t}{l}\right)^2; \qquad I \approx t^4. \tag{2.1}$$

In order to calculate the Young's modulus of the foam (E^*), the linear-elastic deflection (δ) of a

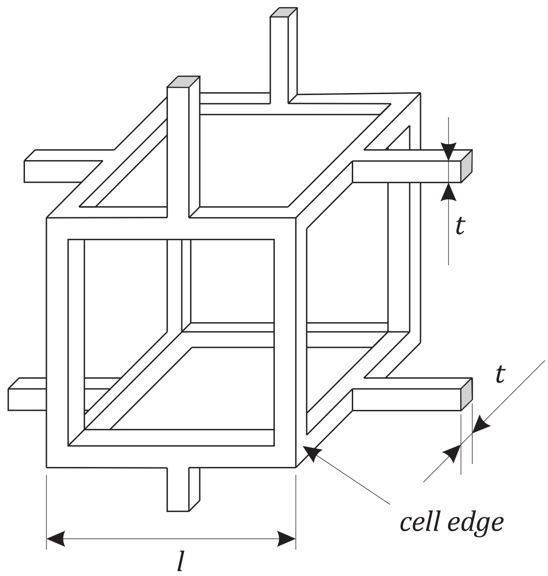

Figure 2.3: The cubic array model for open-cells

beam of length (l) loaded at the midpoint by a load (F) should be determined. According to the standard beam theory

$$\delta = \frac{Fl^3}{E_s I}, \tag{2.2}$$

where the force, (F) is related to the remote compressive stress (σ), whereas deflection (δ) is expressed as the function of strain (ε) using the cubic symmetry: $F = \sigma l^2$; $\delta = \varepsilon l$.

Therefore, the Young's modulus of the foam (E^*) can be determined:

$$E^* = \frac{\sigma}{\varepsilon} = \frac{C_1 E_s I}{l^4}. \tag{2.3}$$

After replacing the relative density (ρ^*/ρ_s) and the second moment area of a member (I), we get

$$\frac{E^*}{E_s} = C_1 \left(\frac{\rho^*}{\rho_s}\right)^2, \tag{2.4}$$

where C_1 is the constant including all geometrical constants. In case of another equiaxed cell shape only this constant changes. As an adequate approximation, $C_1 = 1$ is usually taken.

The shear modulus (G^*) can be calculated similarly. If a shear stress (τ) is applied, the cell members will bend again and the bending deflection (δ) will be the same as at the compressive load. The shearing stress (τ) and strain (γ) can be calculated from the following formulas: $F = \tau l^2$; $\delta = \gamma l$.

Therefore the shear modulus can be determined the following way:

$$G^* = \frac{\tau}{\varepsilon} = \frac{C_2 E_s I}{l^4}, \tag{2.5}$$

from which, replacing the relative density (ρ^*/ρ_s) and the second moment area of a member (I);

$$\frac{G^*}{E_s} = C_2 \left(\frac{\rho^*}{\rho_s}\right)^2, \tag{2.6}$$

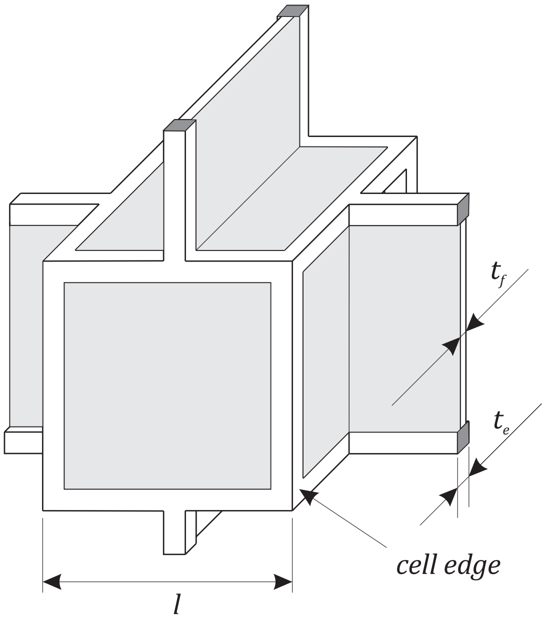

Figure 2.4: The cubic array model for closed-cells

where C_2 is the constant of the geometry and in case of proper approximation: $C_2 = 3/8$.

The last of the moduli, the Poisson's ratio (ν^*) in case of linear-elastic and isotropic material gives the connection between the Young's and the shearing moduli

$$G^* = \frac{E^*}{2(1+\nu^*)}. \tag{2.7}$$

From which expressing the Poisson's ratio (ν^*):

$$\nu^* = \frac{C_1}{2C_2} - 1. \tag{2.8}$$

As it is shown the Poisson's ratio is constant, solely a function of cell geometry and independent of density. In case of approximation: $C_1 = 1$ and $C_2 = 3/8$, thus $\nu^* = 1/3$.

Closed cells

Closed cells polymer foams, which have a substantial fraction of solid in the cell faces, can be modelled as a cube, in which a fraction (ϕ) of solid is contained in the cell edges, with a thickness (t_e); and the remaining $(1-\phi)$ fraction is in the cell-faces with the thickness t_f. These moduli required for describing the linear elasticity of closed cells are the same as the case of open cells (E^*, G^*, ν^*). The moduli can be expressed as the sum of the three mechanisms undergoing in closed cells: cell bending, membrane stretching and gas pressure. The Young's modulus of cell bending and membrane stretching can be determined from the work done against them $\frac{1}{2}F\delta$, which is proportional to

$$\frac{1}{2}F\delta = \alpha\frac{E_s I \delta^2}{l^3} + \beta E_s \delta^2 t_f \ , \tag{2.9}$$

where α and β are constants. Because of $I \approx t_e^4$ and $E^* \approx (F/l^2)/(\delta/l)$:

$$\frac{E^*}{E_s} = \alpha'\frac{t_e^4}{l^4} + \beta'\frac{t_f}{l}. \tag{2.10}$$

The required formula of E^* (expressed in the function of relative density) can be related to this equation

$$\frac{E^*_{bend}}{E_s} = C_1\phi^2\left(\frac{\rho^*}{\rho_s}\right)^2 + C_1(1-\phi)\frac{\rho^*}{\rho_s}, \tag{2.11}$$

where C_1 and C_1' are geometric constants, which can be approximated by $C_1 = C_1' = 1$.

The contriubution to Young's modulus by the pressure of enclosed gas (p) is the result of the cell volume decrease (from V_0 to V) caused by the compression

$$\frac{V}{V_0} = 1 - \varepsilon(1-2\upsilon^*). \tag{2.12}$$

The volume of the enclosed gas (V_g) does not contain the volume of cell edge and faces, thus

$$\frac{V_g}{V_{g0}} = \frac{1-\varepsilon(1-2\upsilon^*) - \frac{\rho^*}{\rho_s}}{1-\frac{\rho^*}{\rho_s}}. \tag{2.13}$$

According to Boyle's law ($pV_g = p_0V_{g0}$), where p is the pressure of the gas inside, the pressure overcome by the compressive stress is $p' = p - p_0$. Therefore the contribution of gas pressure to the Young's modulus is

$$E^*_g = \frac{dp'}{d\varepsilon} = \frac{d\left(\frac{p_0\varepsilon(1-2\upsilon^*)}{1-\varepsilon(1-2\upsilon^*)-\frac{\rho^*}{\rho_s}}\right)}{d\varepsilon} = \frac{p_0(1-2\upsilon^*)}{1-\frac{\rho^*}{\rho_s}}. \tag{2.14}$$

Now, the Young's modulus can be expressed as the sum of the expressions (Eqn. 2.11 and 2.14) listed above and using the recommended constant values ($C_1 = C_1' = 1$):

$$\frac{E^*}{E_s} = \phi^2\left(\frac{\rho^*}{\rho_s}\right)^2 + (1-\phi)\frac{\rho^*}{\rho_s} + \frac{p_0(1-2\upsilon^*)}{E_s(1-\frac{\rho^*}{\rho_s})}. \tag{2.15}$$

The shear modulus besides cell bending depends on cell-face stretching, which leads us to

$$\frac{G^*}{E_s} = C_2\left(\frac{\rho^*}{\rho_s}\right)^2 + C_2'(1-\phi)\frac{\rho^*}{\rho_s}, \tag{2.16}$$

where C_2 and C_2' are geometric constants, which can be approximated by $C_2 = C_2' = 3/8$.

The Possion's ratio similarly to open-cells is the ratio of the two strains, therefore it depends only on the geometry, but not on the relative density. So it can be approximated again by $\nu^* = 1/3$.

2.2.2 Non-linear elasticity and densification

The compression of elastomeric foams shows linear elasticity typically until 5% of strain. At larger strains when the bending turns into buckling, the polymer foam remains elastic, but the stress-strain curve becomes non-linear. At the specific elastic collapse stress (σ^*_{el}) a collapse plateau can be observed.

In case of open-cells, σ^*_{el} can be determined from the critical load, which is according to the Euler-formula,

$$F_{crit} = \frac{n^2\pi^2E_sI}{l^2}. \tag{2.17}$$

The factor n is the number of constraints at the end of the cell edges. The collapse stress σ^*_{el} is proportional to

$$\sigma^*_{el} \approx \frac{F_{crit}}{l^2} \approx \frac{E_s I}{l^4}. \tag{2.18}$$

Substituting the correspondences in Eqn. 2.1, the elastic collapse stress can be expressed as the function of relative density

$$\frac{\sigma^*_{el}}{E_s} = C_4 \left(\frac{\rho^*}{\rho_s}\right)^2, \tag{2.19}$$

where C_4 is the constant of the geometry, with the usual value: $C_4 = 0.05$. If the relative density is higher ($\rho^*/\rho_s > 0.3$) a density correction is added to the formula above

$$\frac{\sigma^*_{el}}{E_s} = C_4 \left(\frac{\rho^*}{\rho_s}\right)^2 \left(1 + \left(\frac{\rho^*}{\rho_s}\right)^{\frac{1}{2}}\right)^2. \tag{2.20}$$

In this case the constant can be approximated by $C_4 = 0.03$.

When the structure is closed, the additional stress by the enclosed gas pressure rises the collapse stress, if the initial pressure of the fluid (p_0) is higher than the atmospheric pressure (p_{at}). In case of man-made foams p_0 is usually equal to p_{at} so the gas do not has a considerable effect on σ^*_{el}, thus the formulas for open-cell (Eqn. 2.19 and 2.20) is valid for closed-cells as well.

After the collapse, the plateau is horizontal when the cell is open. Although having a closed cell foam, the plateau rises due to the enclosed gas, which creates a restoring pressure (p'), which was determined in Eqn. 2.14. In this case $\nu^* \approx 0$, so the curve of the plateau can be expressed as

$$\frac{\sigma^*}{E_s} = 0.05 \left(\frac{\rho^*}{\rho_s}\right)^2 + \frac{p_0 \varepsilon}{E_s(1 - \varepsilon - \frac{\rho^*}{\rho_s})}. \tag{2.21}$$

The last part of the stress-strain curve is the densification, which is described by the limiting strain (ε_d). Above this strain the cell-faces compress each other, and the rise stress-strain curve tends to E_s. The value of the limiting strain was determined experimentally as

$$\varepsilon_d = 1 - 1.4 \left(\frac{\rho^*}{\rho_s}\right). \tag{2.22}$$

2.3 Mechanical properties in tension

Similarly to compression the tensile stress-strain curve can be divided to a linear elastic and a non-linear part. When the strain is small ($\varepsilon < 5\%$) the foam shows linear elasticity, which can be described with the same set of moduli as in case of compression. Even the mechanisms are the same (bending, face stretching, enclosed gas pressure), so the same formulas (2.4, 2.6 and 2.15, 2.16) are valid for open-cell and closed cell tension.

At larger strains the stiffness of elastomeric foams increases and the stress-strain curve becomes non-linear. In this case the cell edges originally lying at an angle to the tensile axis rotates towards it, which decreases the moment of bending. Thus bending is replaced by stretching as the dominating mechanism of the deformation. This non-linear behaviour for uniaxial tension is described by the formula

$$\frac{\sigma^*}{E_s} = 1.1 \left(\frac{\rho^*}{\rho_s}\right)^2 \varepsilon + 3.74 \left(\frac{\rho^*}{\rho_s}\right)^3 \varepsilon^2 + 0.0343 \left(\frac{\rho^*}{\rho_s}\right) \varepsilon^3. \tag{2.23}$$

3
Measurements

3.1 Introduction

The aim of the thesis is to investigate the effect of surface skin layer on the mechanical behaviour. The mechanisms presented in *Chapter 2* only describe the behaviour in case of homogenous material properties. Nevertheless, due to the manufacturing circumstances all polymer foam contains a surface skin layer, which results in an inhomogeneous material structure (Figure 3.1).

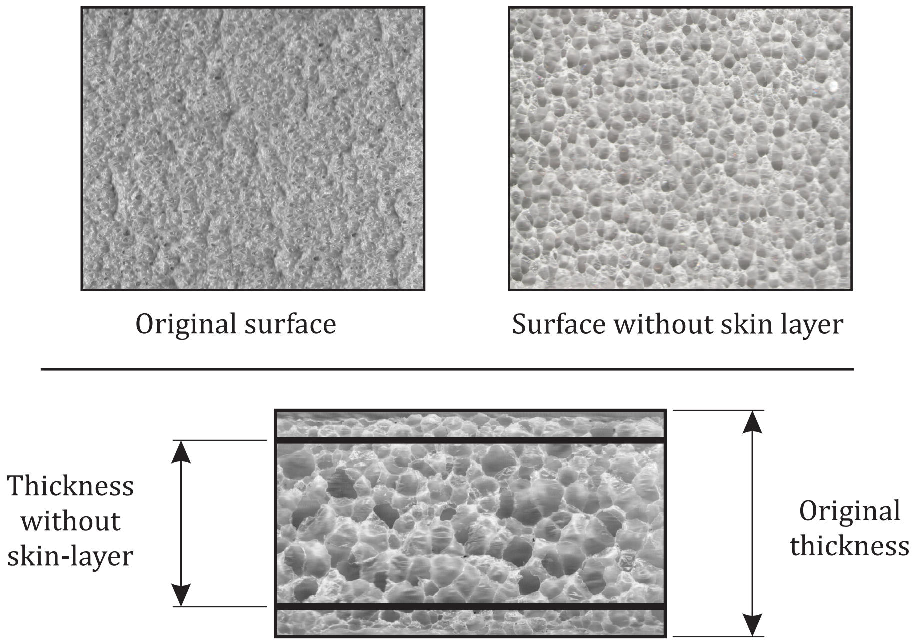

Figure 3.1: The skin layer of polymer foams

In order to determine the effect of skin layer, mechanical tests have been executed on a specific polyethylene closed-cell polymer foam, whose material properties are contained in the following table (Table 3.1).

Material	Polyethylene
Density of the cellular material (ρ_s)	922 kg/m^3
Density of the foam (ρ^*)	40.521 kg/m^3
Realtive density (ρ^*/ρ_s)	0.043949
Thickness	13 mm

Table 3.1: Material properties of the tested polymer foam

The goal of tests is to determine the stress-strain curves of the polymer foam in all directions with and without the surface skin layer in case of uniaxial load, thus the effect of it can be determined by analysing the curves. The directions are indexed according to the manufacturing directions:

- Machine direction (MD)
- Non-machine direction (NMD)
- Thickness (T)

As the whole stress-strain curve cannot be measured at once, necessarily the tensile and compression part of it have been determined separately by tensile and compression tests. In order to measure the mechanical properties of the foam without skin layer, all tests needed to be executed with skin-layer-free specimens as well. Therefore the experimental investigation was set up by the following tests, which are denoted by the codes in bracket:

1. Compression test (C)
   (a) Machine direction with layer (C-MD)
   (b) Machine direction without layer (C-MD-WL)
   (c) Non-machine direction with layer (C-NMD)
   (d) Non-machine direction without layer (C-NMD-WL)
   (e) Thickness with layer (C-T)
   (f) Thickness without layer (C-T-WL)
2. Tensile test (T)
   (a) Machine direction with layer (T-MD)
   (b) Machine direction without layer (T-MD-WL)
   (c) Non-machine direction with layer (T-NMD)
   (d) Non-machine direction without layer (T-NMD-WL)

The skin-layer-free specimens could be created by removing an approximately 1.7 mm thick skin-layer from both sides of the foam (see Figure 3.1). Towards that, a slicer device has been designed and produced according to the recommendation of the D-3576 98 standard of the American Society for Testing and Materials (ASTM) [9]. The slice of skin layer was removed by a commercial cutting blade moving on a specific sliding assembly (Figure 3.2), while the specimen was placed between the sliding assembly, which fixes the position of the specimen. The thickness of the sliced skin layer could be adjusted by putting the required amount of slip of paper under the specimens.

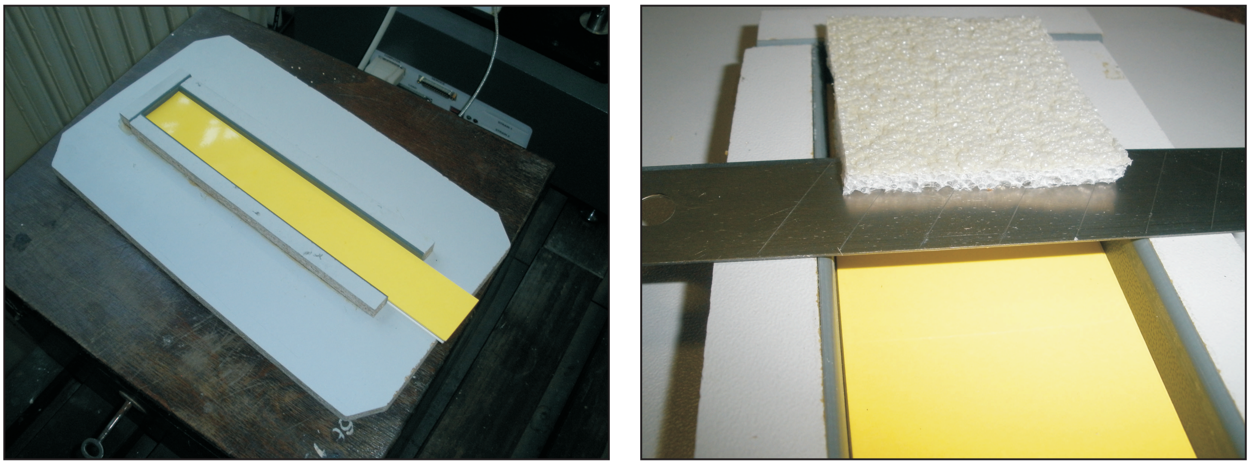

Figure 3.2: The slicer device for removing surface skin layer

The tensile and compression tests have been executed in the laboratory of the Department of Applied Mechanics of BME, on an INSTRON 3345 Single Column Universal Testing System for Low-force.

In order to receive a comparable result for all tests, the speed of deformation ($\dot{\varepsilon}$) should be equal in all cases. The deformation speed can be determined by

$$\dot{\varepsilon} = \frac{v}{L_0}, \tag{3.1}$$

where v is the speed of the crosshead, L_0 is the initial length. Due to having an adequately slow deformation, the value of $\dot{\varepsilon}$ was chosen for

$$\dot{\varepsilon} = 0,015\frac{1}{\mathrm{s}} = 0,9\frac{1}{\mathrm{min}}. \tag{3.2}$$

Therefore the crosshead speed of each tests was determined as

$$v = 0.9L_0. \tag{3.3}$$

During the measurements, the Testing System recorded the load (F) and the displacement (ΔL). Simultaneously, the cross-direction stretches (λ_2, λ_3) were recorded using a full-HD camera and evaluated by further image processing.

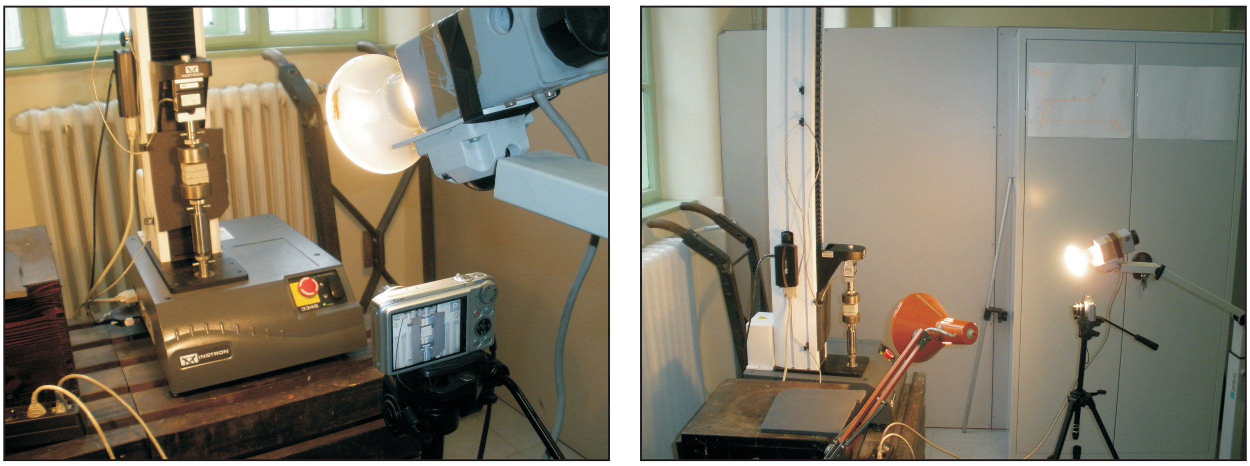

Figure 3.3: The Testing System and the measurement layout

3.2 Compression tests

3.2.1 Description of the test, geometry of specimens

When the mechanical test is compression, a compression platen system should be fixed to the Testing System, which compresses the specimens placed on the lower platen. The initial separation (Figure 3.4) of platens is H_0, and the compressive length of specimens is L_0. After starting the test the higher platen moves with constant velocity, which was adjusted according to Eqn. (3.2) and (3.3). The test stops, when the the platens are very close to each other, or when F reaches a critical value (3000 N).

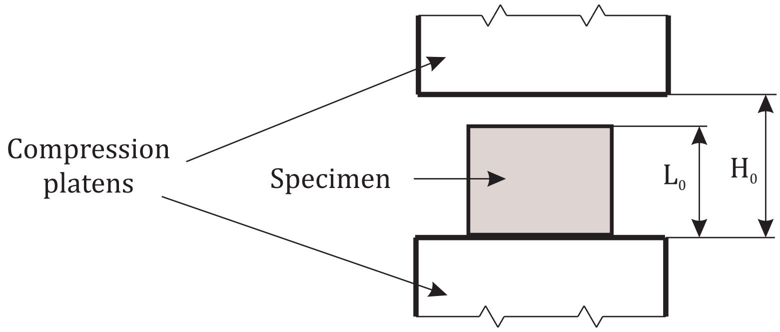

Figure 3.4: The layout of compression test

Specimens

The geometry of specimens used in compression test is based on the recommendation of ISO-3386-1 standard of the International Organization for Standardization (ISO) [7]. According to the standard the specimen is required to be right parallelepiped with a minimum width/thickness ratio of 2:1. The optimal thickness is 50 mm, although having a thinner sheet of foam, specimens can be plied together. Besides, the area of specimen should be as big as possible, but it should not overlap the compression platen. In our case the diameter of the compression platen is 57 mm, so the maximum width of the specimen is approximately 40 mm.

- Machine direction (MD)

  In order to avoid the buckling of the specimen, three of them were fixed next to each other, therefore the area became square. Naturally when the specimen is skin-layer-free, the width of the thickness direction is less.

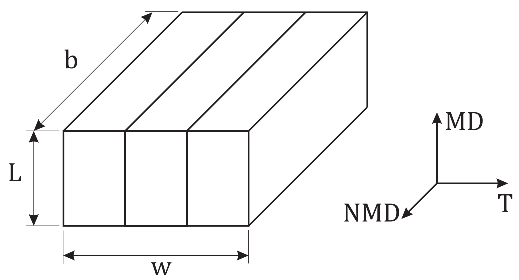

Figure 3.5: Geometry of specimens for MD compression

After cutting and fixing the specimens, the final dimensions of each specimens have been measured, which is enclosed in Table 3.2.

Code	L [mm]	w [mm]	b [mm]	A [mm^2]
C-MD-01	18	35.8	39	1396.2
C-MD-02	19.6	36.5	39	1423.5
C-MD-03	20.3	38.5	39	1501.5
C-MD-04	19.5	38	39	1482
C-MD-05	19.7	37	39	1443
C-MD-06	18.5	37	39	1443
C-MD-WL-07	19.6	38.5	24.5	943.3
C-MD-WL-08	19.1	39.5	23.1	912.5
C-MD-WL-09	19.4	37.5	24.6	922.5
C-MD-WL-10	18.8	36.5	25.1	916.2
C-MD-WL-11	19.7	37	23.5	869.5
C-MD-WL-12	19.3	36.5	24.5	894.3

Table 3.2: Dimensions of specimens for MD compression

- Non-machine direction (NMD)

  The geometry of specimens is similar to machine direction's and test pieces were fixed next to each other as well. The geometrical structure and data of NMD specimens are displayed in Figure 3.6 and Table 3.3.

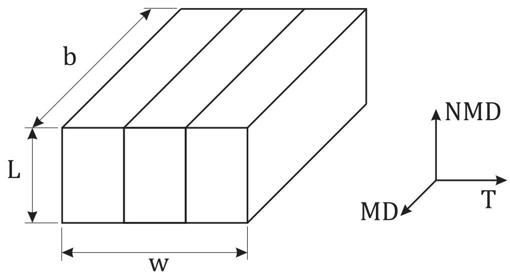

Figure 3.6: Geometry of specimens for NMD compression

Code	L [mm]	w [mm]	b [mm]	[mm^2]
C-NMD-01	18.5	37.5	39	1462.5
C-NMD-02	19.5	37.5	39	1462.5
C-NMD-03	18.5	38	39	1482
C-NMD-04	20.4	37.5	39	1462.5
C-NMD-05	19.6	36	39	1404
C-NMD-06	19.7	38	39	1482
C-NMD-WL-07	18.5	38	24.5	931
C-NMD-WL-08	21.8	36.5	25.4	927.1
C-NMD-WL-09	19.2	37.5	25.1	941.3
C-NMD-WL-10	18.8	36.5	25.7	938.1
C-NMD-WL-11	18.5	37.5	25.4	952.5
C-NMD-WL-12	18.9	37	24.6	910.2

Table 3.3: Dimensions of specimens for NMD compression

- Thickness

  When the direction of compression is thickness, the basis of specimen is a square (39×39). Purposely having a more optimal specimen, three specimens were plied together, so finally a cubic test piece was received.

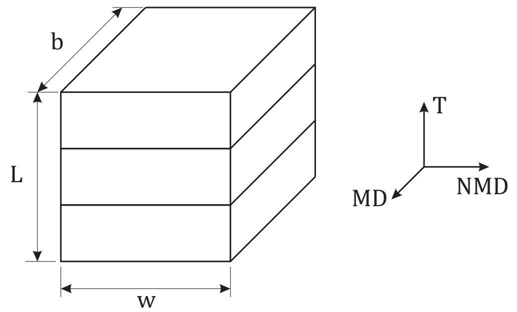

Figure 3.7: Geometry of specimen for thickness compression

Code	L [mm]	w [mm]	b [mm]	A [mm^2]
C-T-01	39	38	37	1406
C-T-02	39	38	39.5	1501
C-T-03	39	39	38.5	1501.5
C-T-04	39	39	38	1482
C-T-05	39	37.5	37,5	1406.3
C-T-06	39	36.5	38	1387
C-T-WL-07	23.6	38.5	38	1463
C-T-WL-08	23.2	39	38.5	1501.5
C-T-WL-09	23.4	39.5	38.5	1520.8
C-T-WL-10	23.8	38	39.5	1501
C-T-WL-11	23.8	38	36.5	1387
C-T-WL-12	23.9	38.5	38.5	1482.3

Table 3.4: Dimensions of specimens for thickness compression

Hereafter the indices of the directions are the following:

1. - longitudinal (compression) direction (L)
2. - cross-direction of width (w)
3. - cross-direction of length (b)

Evaluation

The process of evaluation was done in *Wolfram Mathematica 7* [18] and *Microsoft Excel 2010* [14]. The *Mathematica* notebooks are enclosed in the `Appendix`. As a result of the compression test, the load-displacement ($F - \Delta L$) diagram and the video of the cross-direction stretches were given. Firstly, the starting point of the compression curve should be found, where the higher platen touches the specimen. It can be determined by a minimal limit of load ($F_0 < 0.5$ N), because before that point the higher platen do not touches the specimen, so the load is zero. The point, when the load reaches 0.5 N should be the starting point (L_1), the previous part of the curve should be dropped. From the starting point the accurate compression length (L_0) of the specimen could be determined as $L_0 = H_0 - L_1$ (Figure 3.4). Due to the specimen plying, the initial part of the linearly elastic period is non-linear, so an inflection point can be observed on the stress-strain curve. This inflection point was detected by the local extreme value of the first derivation of the curve. The initial non-linear region before the inflection point was replaced by a linear session (Figure 3.8). From the processed $(F - \Delta L)$ curve the stress-stretch characteristic $(P_1 - \lambda_1)$ can be determined. The stress is given in the so-called engineering-stress (P) form

$$P_1 = \frac{F}{A_0}, \tag{3.4}$$

which means that the load (F) applied to the specimen is divided by the initial cross-sectional area of the specimen (A_0). The stretch was determined by

$$\lambda_1 = \frac{\Delta L + L_0}{L_0} = \frac{\Delta L}{L_0} + 1. \tag{3.5}$$

After having the stress-stretch characteristics of the specimens with and without skin layer, the effect of the layer could be demonstrated by comparing the mean of the curves in both cases.

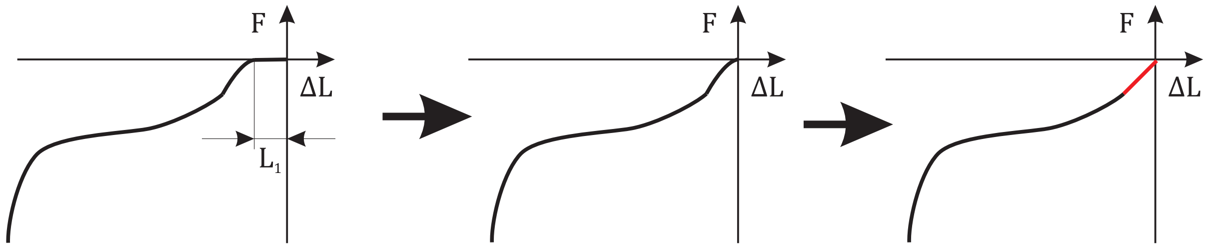

Figure 3.8: The post-processing of compression test results

The cross-direction stretches (λ_2, λ_3) were determined by cropping a small slice of the video (Figure 3.9), showing the side of the test piece, which underwent video processing in *VirtualDub* [12], a freeware video editor by using "treshhold" filter. As a result, a black and white video was received, where the specimen is white and the environment is black. The area of the white part divided by the white area of the first frame gives an averaged cross-direction stretch over the sides of the specimens in every frame. The calculations were completed in *MatLab* [13]. After converting the number of frames into time (frame rate of the camera is 23.976 frame/sec) the cross-direction stretches can be determined in terms of the longitudinal stretch.

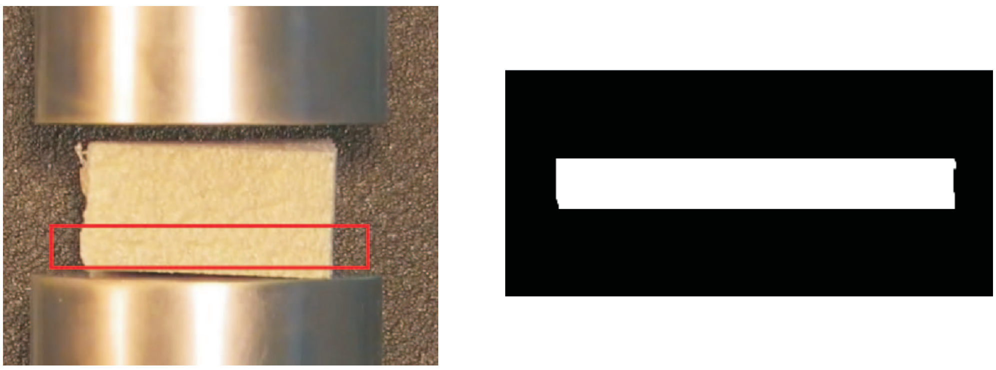

Figure 3.9: The process of creating black and white picture from the video of compression tests

At the end of the evaluation of measured data in case of compression test, the following results were received for of all directions:

- stress-stretch characteristic ($P_1 - \lambda_1$) with and without layer,
- comparison of stress-stretch characteristic ($P_1 - \lambda_1$),
- the cross-direction stretches in terms of the longitudinal stretch ($\lambda_1 - \lambda_2$) and ($\lambda_1 - \lambda_3$).

3.2.2 Machine direction

The compression test in machine direction was executed on $4 - 4$ specimens with and without skin layer, respectively (Figure 3.10). The parameters of the test are listed in Table 3.5. During the test, in order to determine the relation of longitudinal and cross-direction stretches, one side of the specimen was video-recorded, so we received the series of data of each cross-directions at each type of specimens.

H_0	29 mm
L_0	$\sim$ 23.5 mm
v	21.15 mm/min

Table 3.5: Parameters of C-MD tests

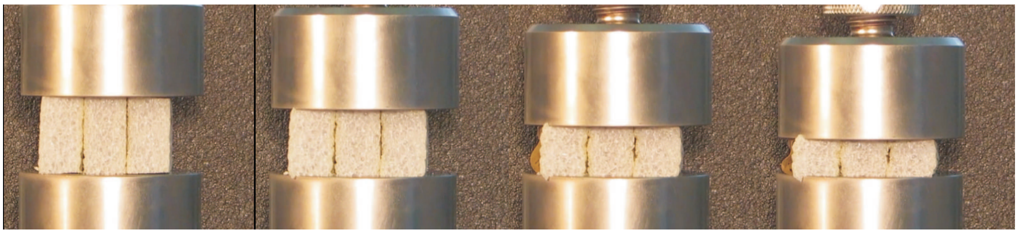

Figure 3.10: The process of machine direction compression

The post-processed stress-stretch curves ($P_1 - \lambda_1$) of the specimens with and without skin layer are displayed in Figures 3.11 and 3.12. As it is seen, the trend of the curves is similar, all the regimes described in *Chapter 2* (linear elasticity, collapse plateau and densification) can be observed.

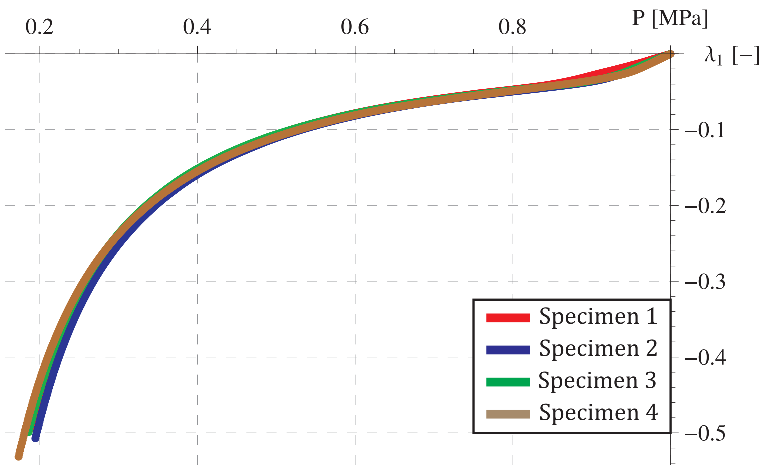

Figure 3.11: The stress-stretch curve of C-MD specimens

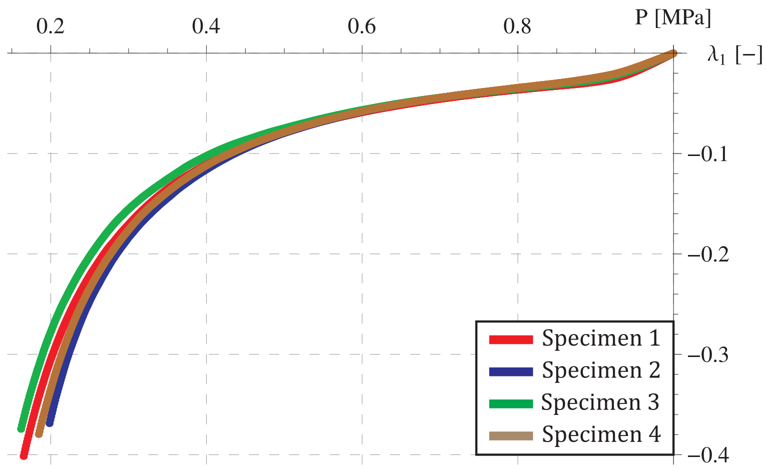

Figure 3.12: The stress-stretch curve of C-MD-WL specimens

By comparing the mean of the stress-stretch curves of all types, the effect of skin layer is visualized (Figure 3.13). In case of layer-free specimens, the stresses are lower, which means that, the polymer foam without skin layer is more compressible and more flexible. The initial slope is smaller, because the foam became more flexible.

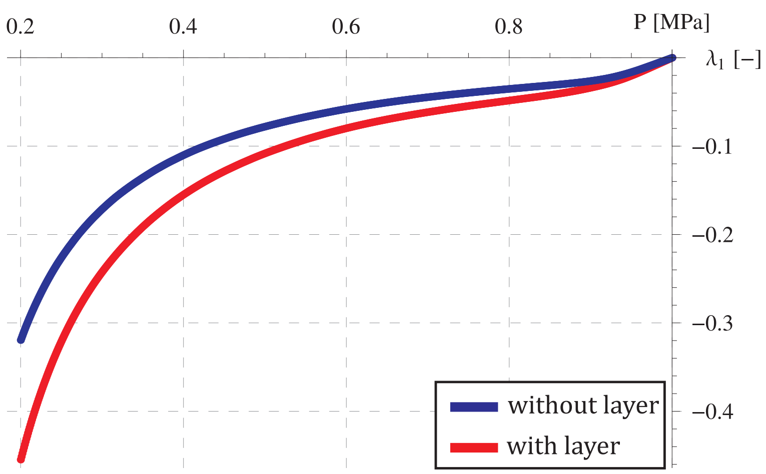

Figure 3.13: The comparison of C-MD specimens' stress-stretch curve with and without layer

The relation of stretches contains lot of disturbance, caused by the error of the video-processing and the geometrical inaccuracy of specimens (Figures 3.14 and 3.15). However, the tendency, especially at higher stretches ($\lambda_1 < 0.5$), shows that during the compression the cross-direction stretches increases.

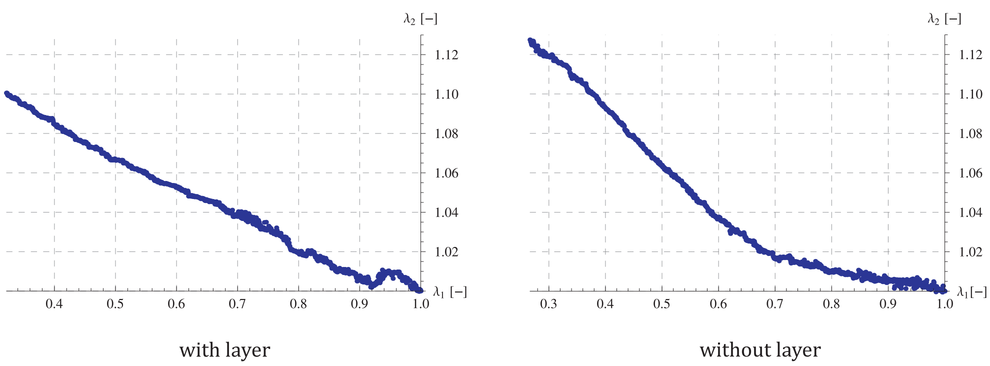

Figure 3.14: The relation between stretches (λ_1, λ_2) of C-MD specimens with and without layer

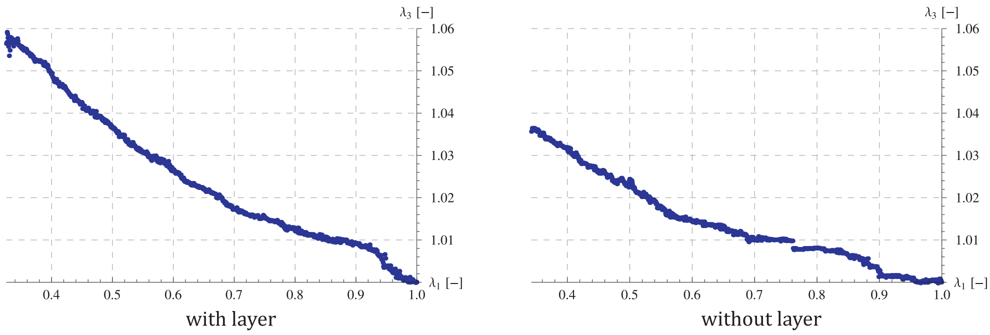

Figure 3.15: The relation between stretches (λ_1, λ_3) of C-MD specimens with and without layer

3.2.3 Non-machine direction

The execution of non-machine direction compression test was similar to the MD test, we used the same parameters (Table 3.6) and number of specimens (Figure 3.16). The results (Figures 3.17, 3.18, 3.19, 3.20 and 3.21) became really similar as well, but unfortunately the relation of stretches contains much more disturbance.

H_0	29 mm
L_0	~ 23.5 mm
v	21.15 mm/min

Table 3.6: Parameters of C-NMD tests

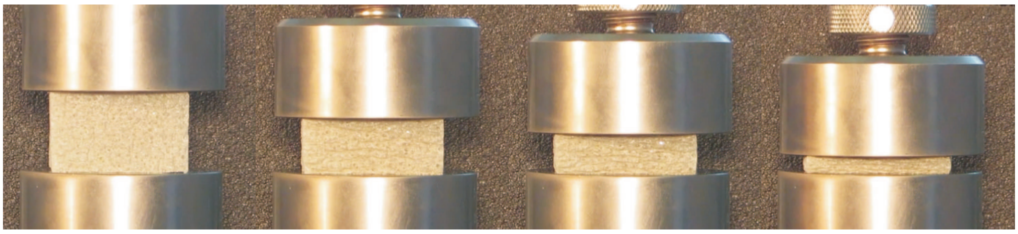

Figure 3.16: The process of non-machine direction compression

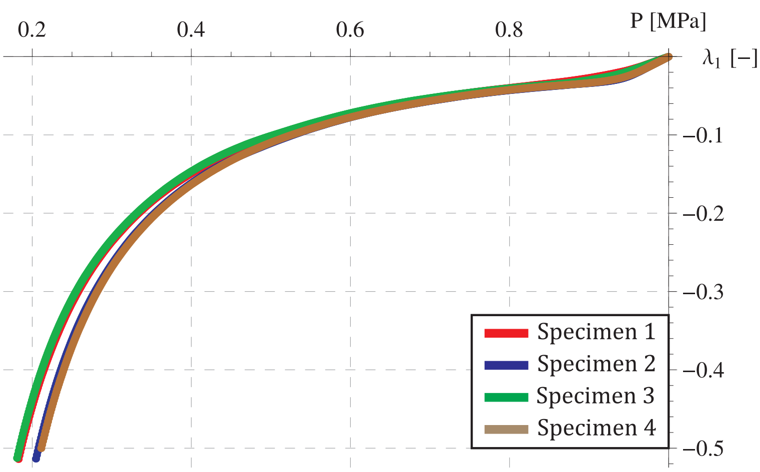

Figure 3.17: The stress-stretch curve of C-NMD specimens

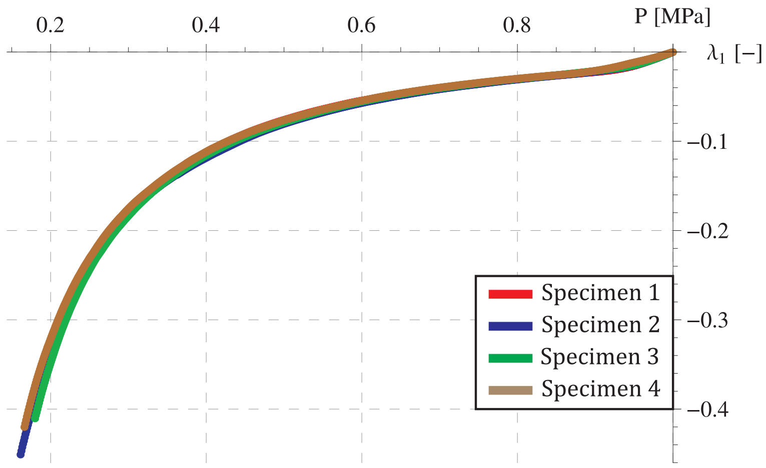

Figure 3.18: The stress-stretch curve of C-NMD-WL specimens

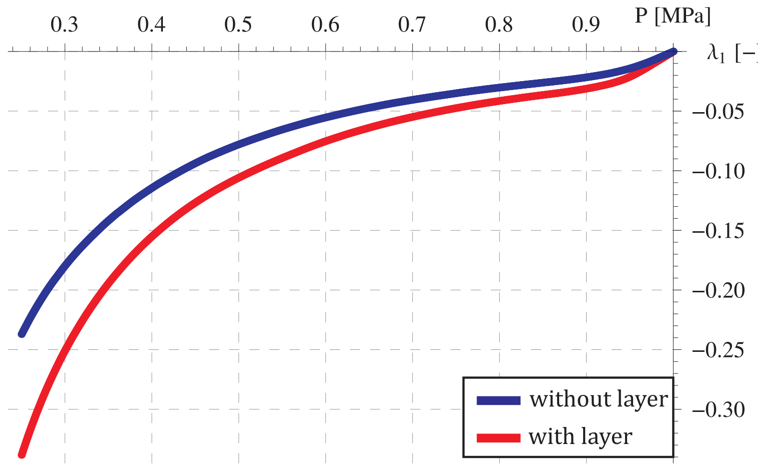

Figure 3.19: The comparison of C-NMD specimens' stress-stretch curve with and without layer

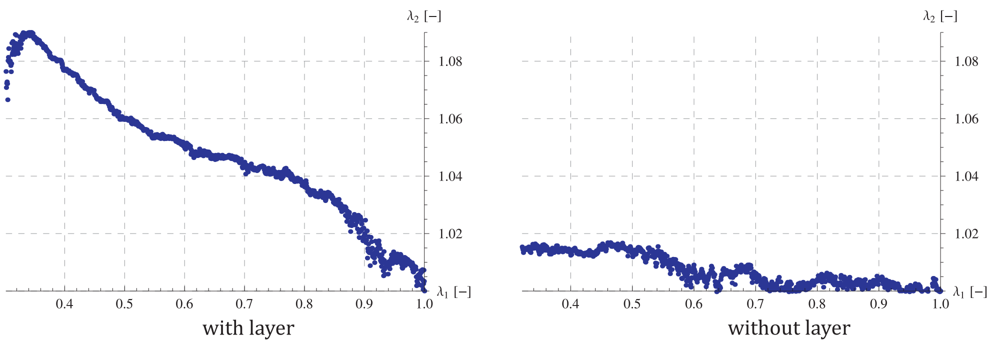

Figure 3.20: The relation between stretches (λ_1, λ_2) of C-NMD specimens with and without layer

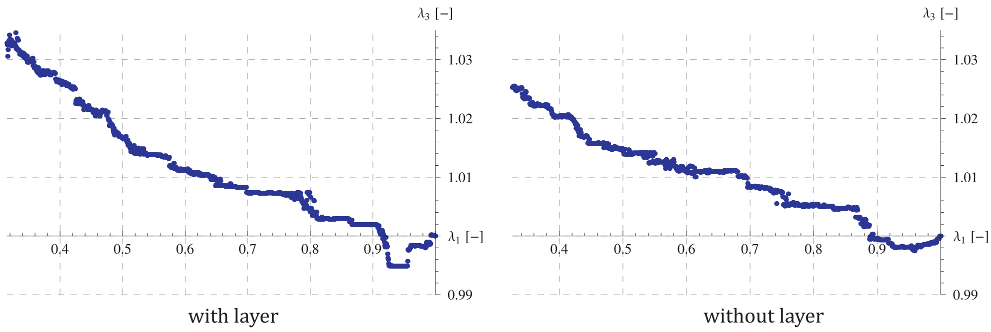

Figure 3.21: The relation between stretches (λ_1, λ_3) of C-NMD specimens with and without layer

3.2.4 Thickness

When the direction of compression is thickness, the compression length of specimens with and without layer is different, so the parameters of the test depend on the type of specimen. (Table 3.7). In this case we used 4 specimens per each type as well.

With layer (C-T)		Without layer (C-T-WL)	
H_0	42 mm	H_0	29 mm
L_0	$\sim$ 39 mm	L_0	$\sim$ 23.5 mm
v	35.1 mm/min	v	21.15 mm/min

Table 3.7: Parameters of C-T tests

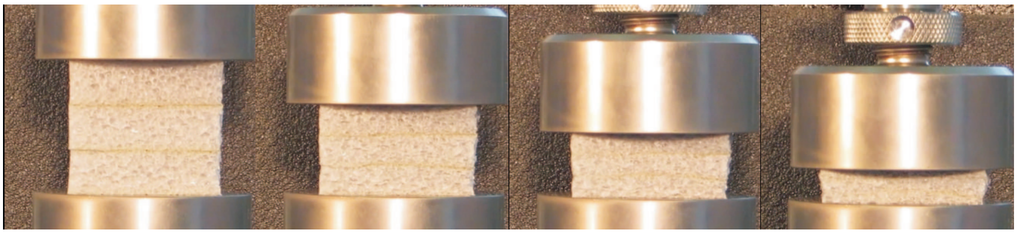

Figure 3.22: The process of thickness direction compression

The results (Figures 3.23, 3.24, 3.25 and 3.26) show again, that the layer-free specimens are more compressible and more flexible, although the difference between the two types is smaller. Because of the geometry of specimens in this case the two cross-direction stretches are considered to be equal ($\lambda_2 = \lambda_3$), therefore only one cross-direction stretch (λ_2) was measured.

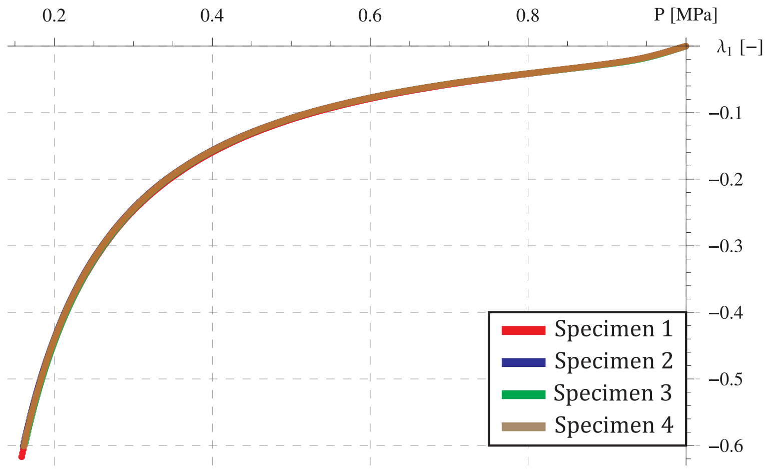

Figure 3.23: The stress-stretch curve of C-T specimens

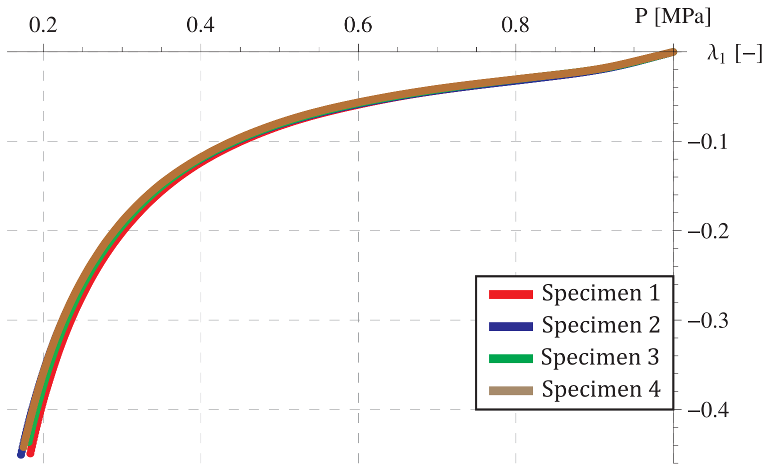

Figure 3.24: The stress-stretch curve of C-T-WL specimens

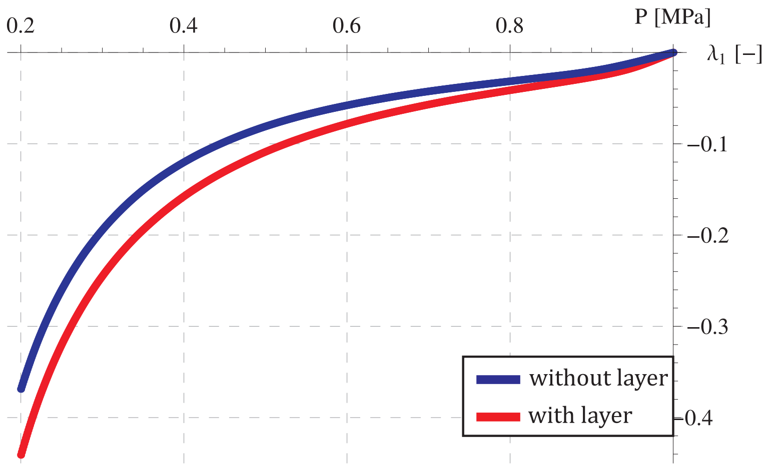

Figure 3.25: The comparison of C-T specimens' stress-stretch curve with and without layer

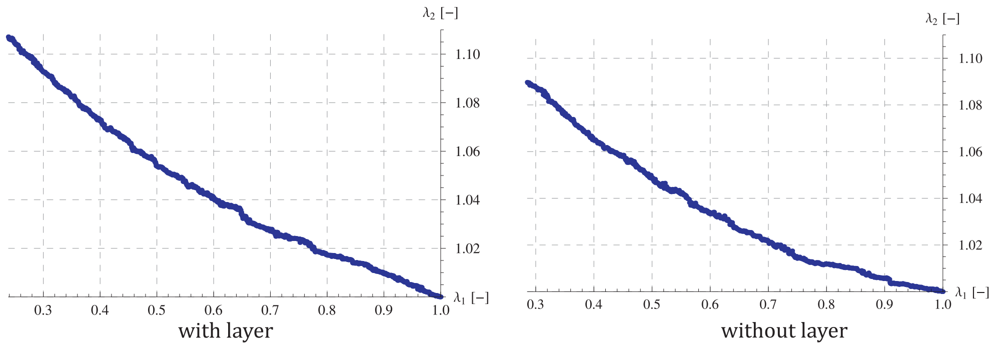

Figure 3.26: The relation between stretches (λ_1, λ_2) of C-T specimens with and without layer

3.2.5 Summary

As the result of compression test shows, the surface skin layer of the polymer foam makes it a bit less compressible and at the initial part less flexible. This can be explained by the increase of relative density (ρ^*/ρ_s) in the skin layer. All material properties described in *Chapter 2*, can be expressed in term of relative density, which leads to the increase of the elasctic modulus (E^*), the elastic collapse stress (σ^*_{el}) and the gradient of the plateau (Eqn. 2.15, 2.19 and 2.21).

Besides, it can be observed that, the skin layer has bigger effects on the behaviour of compression in case of machine and non-machine directions. In these cases the longitudinal direction is parallel with the skin layer, therefore changes the properties of cell-wall buckling. When the compression direction is thickness, the skin layer is perpendicular to the longitudinal direction, so the effect is less considerable.

3.3 Tensile tests

3.3.1 Description of the test, geometry of specimens

After the compression part of the stress-strain characteristic had been determined, tensile tests were executed. In this case, screw side action grips should have been placed in the Testing System, which fixed the specimens. The layout of the tensile measurement and the initial separation (H_0) are shown in Figure 3.27. When the test starts, the top grip starts to move with constant velocity according to Eqn. (3.2). The test stops when the specimen fractures, which is detected by the fall of the load.

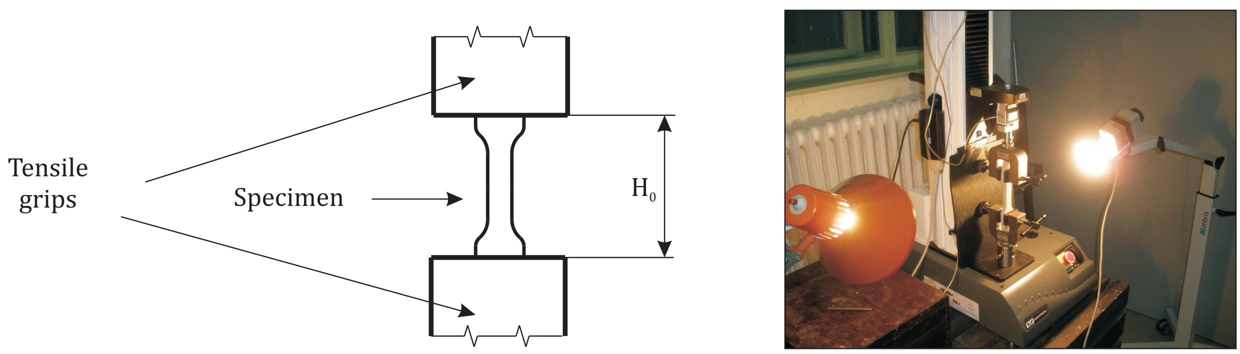

Figure 3.27: The layout of tensile test

Specimens

The geometry of specimens are based on the recommendation on tension specimens of D 3574 03 standard of the American Society for Testing and Materials (ASTM) [8]. The geometry was enlarged proportionately in order to fit into the slicer device (Figure 3.28).

The specimens were cut by laser at the Department of Machine and Product Design at BME by the help of János Szücs (laboratory engineer at the Department of Machine and Product Design), which is highly appreciated. The laser cut was based on the CAD sketch of the specimens.

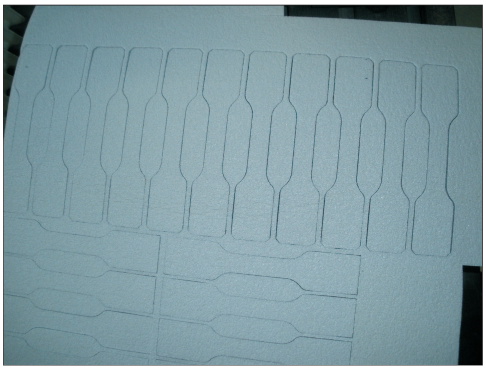

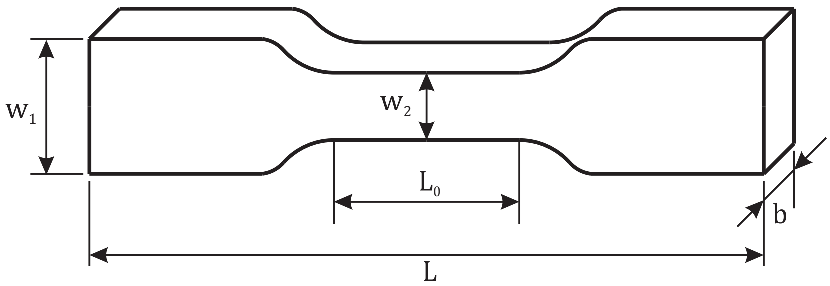

Figure 3.28: The geometry of tensile specimen

L	200 mm
w_1	39 mm
w_2	19 mm
L_0	55 mm
Thickness	13 mm
Thickness (without layer)	9.5 mm
A_0	247 mm^2
A_0 (without layer)	180.5 mm^2

Table 3.8: Dimensions of tensile test specimen

Hereafter the indices of the directions are the following:

1. - longitudinal (compression) direction (L)
2. - cross-direction of width (w)
3. - cross-direction of thickness (b)

Evaluation

As a result of the tensile test the load (F) – displacement (ΔL) diagram was received from the Testing System. This data was post-processed in *Wolfram Mathematica* [18] and *Excel 2010* [14]. The *Mathematica* notebooks are enclosed in the `Appendix`. The initial load (F_0) was subtracted, so the curve starts from 0 N. After the maximum load was determined, all further measurement points were eliminated. From ($F - \Delta L$) curve the stress-stretch ($P_1 - \lambda_1$) curve for tensile was determined according to the expressions in Eqn. 3.4 and 3.5. The effect of skin layer in case of tension was demonstrated again by comparing the mean of the stress-stretch curves with and without skin layer.

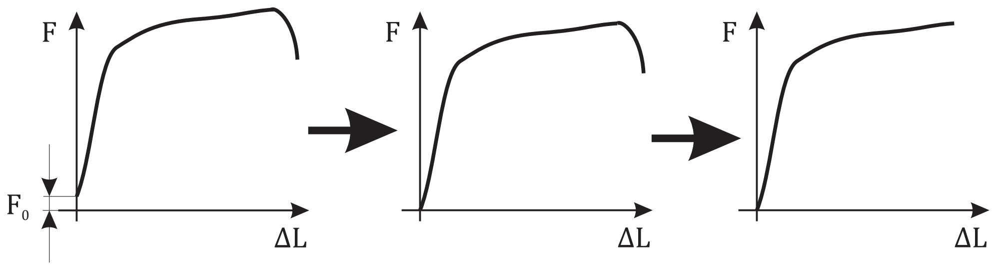

Figure 3.29: The post-processing of tensile test results

The tests were recorded again, so the cross-direction stretches (λ_2, λ_3) in case of all type of specimens could be determined by video processing. Similarly to the compression test, the video was converted to black-and-white in *VirtualDub* [12] (Figure 3.30), and the stretch was given by the ratio of the actual and the initial area of the white part in every frame in *MatLab* [13]. Therefore the cross-direction stretches could be defined in the terms of the longitudinal stretch ($\lambda_1 - \lambda_2, \lambda_1 - \lambda_3$).

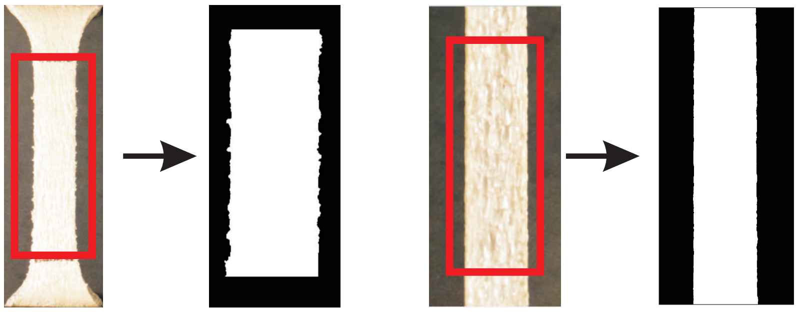

Figure 3.30: The process of creating black and white picture from the video of tensile tests

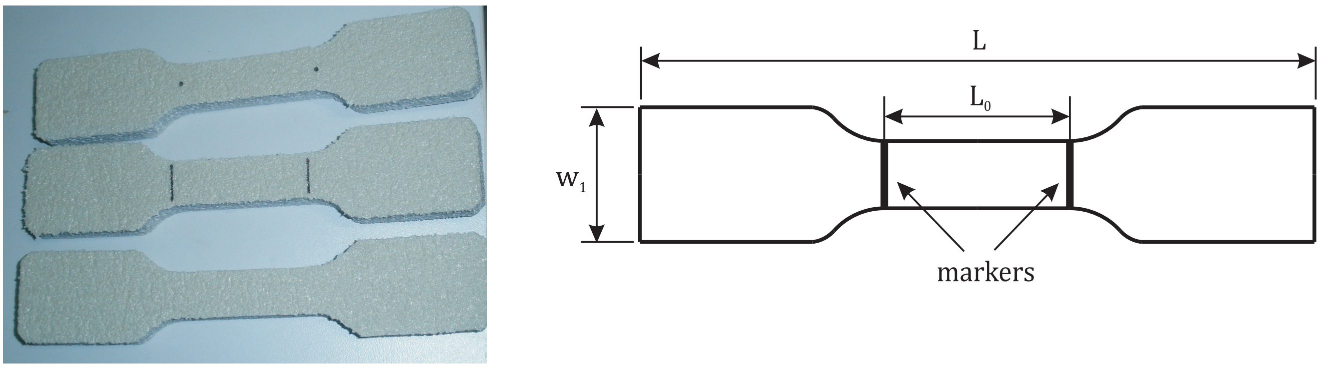

Figure 3.31: Tensile test specimens with markers

Besides, on some specimens markers were placed (Figure 3.31). Thus, during the video processing the longitudinal stretch (λ_1) could be determined independently to the testing machine. Firstly the distance of edges of the grips was tracked in *Adobe AfterEffects* [21], which should give the same results for longitudinal stretch as the Test System. Secondly, the markers were tracked, which gives the accurate stretch of the gauge length, reducing the effect of the shoulders, which can cause errors during the hyperelastic model fitting. After the analysis of the longitudinal stretch from the crosshead (λ_{CH}) and the stretch calculated from markers (λ_M) a correction factor (c) could be determined. The calculation of the correction factor can be found in *Chapter 4*.

At the end of the evaluation of measured data, the following results were received in case of all directions:

- stress-stretch characteristic ($P_1 - \lambda_1$) with and without layer,
- comparison of stress-stretch characteristic ($P_1 - \lambda_1$),
- the cross-direction stretches in terms of the longitudinal stretch ($\lambda_1 - \lambda_2$) and ($\lambda_1 - \lambda_3$),

3.3.2 Machine direction

During the tensile machine direction test $4-4$ specimens were used with and without layer as well (Figure 3.32). The parameters of the test are displayed in Table 3.9. Similarly to compression test the sides of the specimens were video recorded in order to determine the relation of longitudinal stretch (λ_1) and cross-direction stretches (λ_2, λ_3) of both type of specimens.

H_0	90 mm
L_0	$\sim$ 55 mm
v	49.5 mm/min

Table 3.9: Parameters of T-MD tests

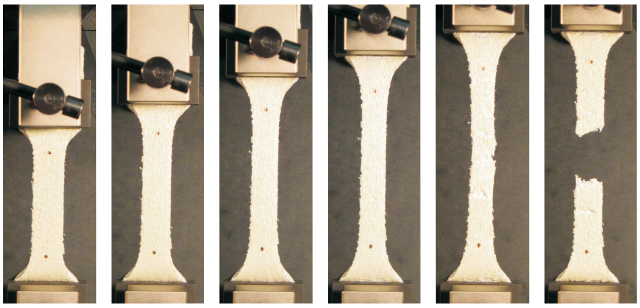

Figure 3.32: The process of machine direction tension

As the stress-stretch ($P - \lambda_1$) curves show, the regimes of tension described in *Chapter 2* can be observed: the initial linearly elastic and the non-linear regime until the fracture.

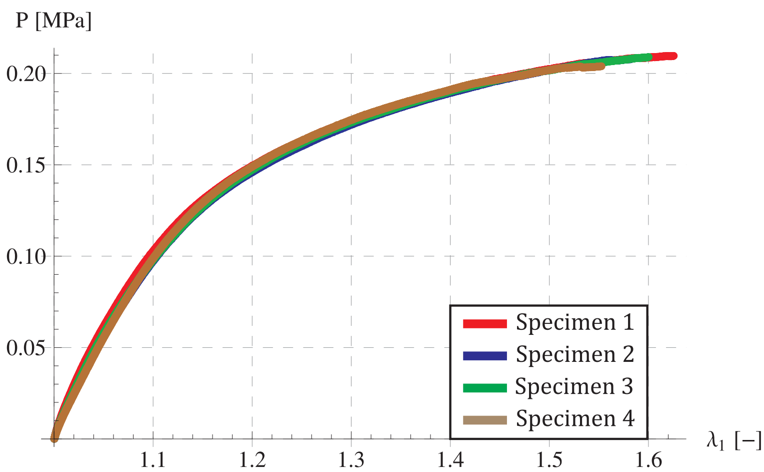

Figure 3.33: The stress-stretch curve of T-MD specimens

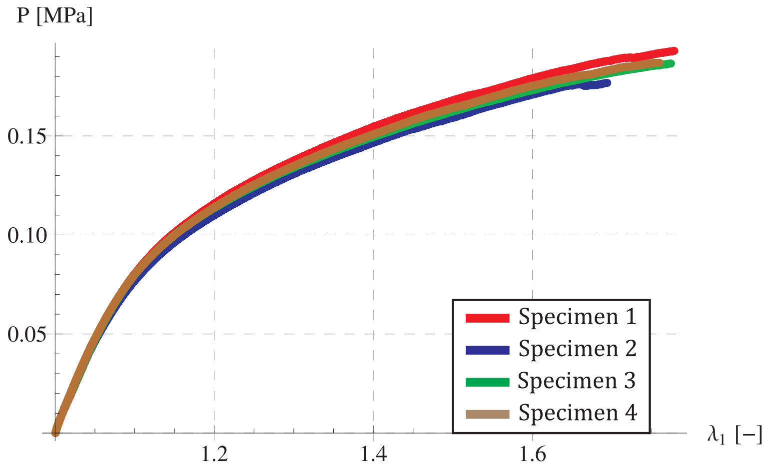

Figure 3.34: The stress-stretch curve of T-MD-WL specimens

The comparison of the mean stress-stretch curves (Figure 3.35) shows, that specimens with skin layer are more fragile. The initial slope of the curve (E^*) and the tensile strength ($\sigma_{\max}$) is higher, while the maximum stretch ($\lambda_{\max}$) is lower.

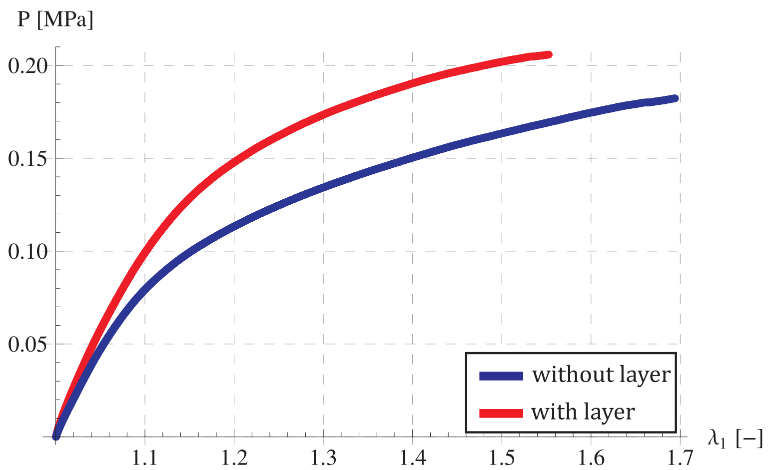

Figure 3.35: The comparison of T-MD specimens' stress-stretch curve with and without layer

From relation of stretches, determined from the video analysis (Figures 3.36, 3.37 and 3.38) it can be noticed, that the cross-direction stretches decreases, while the longitudinal stretch increases during the test, so they are inversely proportional.

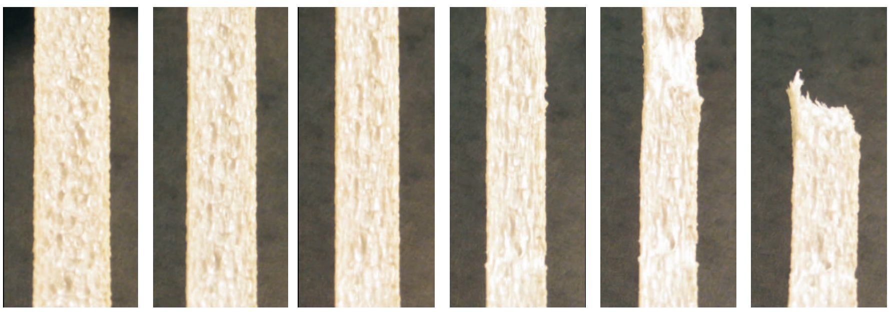

Figure 3.36: The process of cross-direction stretch change during MD tensile test

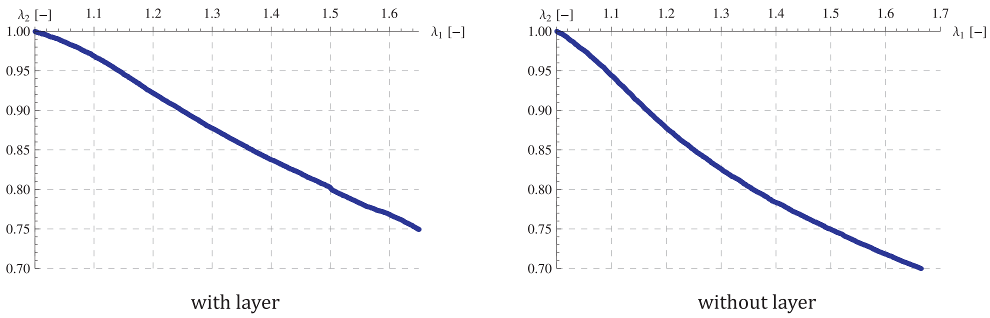

Figure 3.37: The relation between stretches (λ_1, λ_2) of T-MD specimens with and without layer

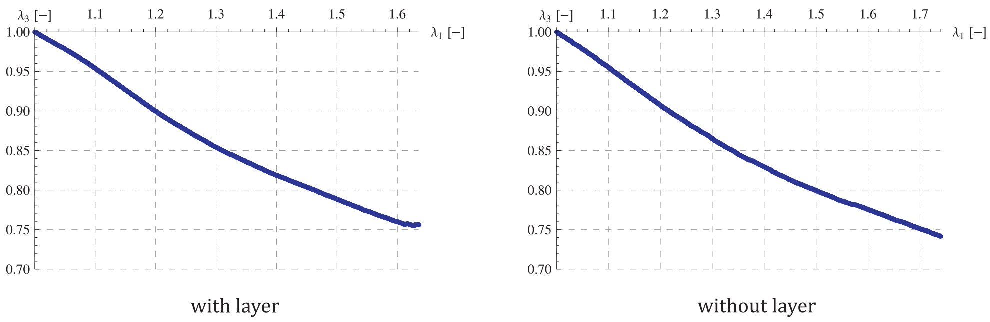

Figure 3.38: The relation between stretches (λ_1, λ_3) of T-MD specimens with and without layer

3.3.3 Non-machine direction

The non-machine direction tensile test is really similar to the machine direction test. We used the same test parameters (Table 3.10), and the results shows the same tendency in point of stress-stretch curves (Figures 3.39, 3.40 and 3.41) and the characteristic of cross-direction stretches (Figures 3.42 and 3.43) in the function of the longitudinal stretch.

H_0	90 mm
L_0	$\sim$ 55 mm
v	49.5 mm/min

Table 3.10: Parameters of T-NMD tests

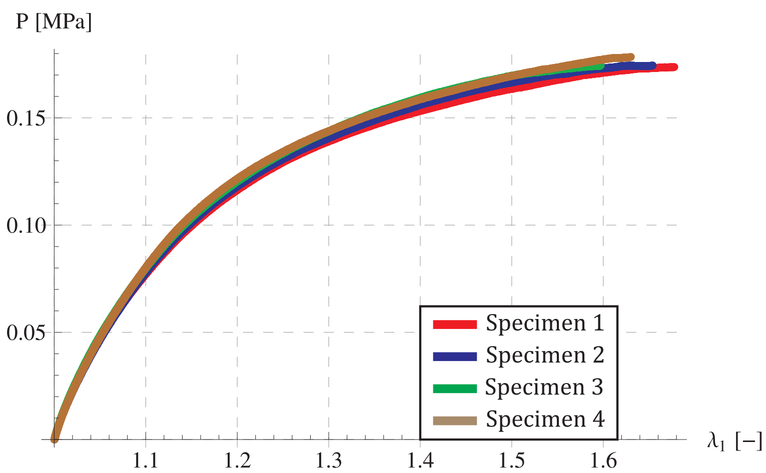

Figure 3.39: The stress-stretch curve of T-NMD specimens

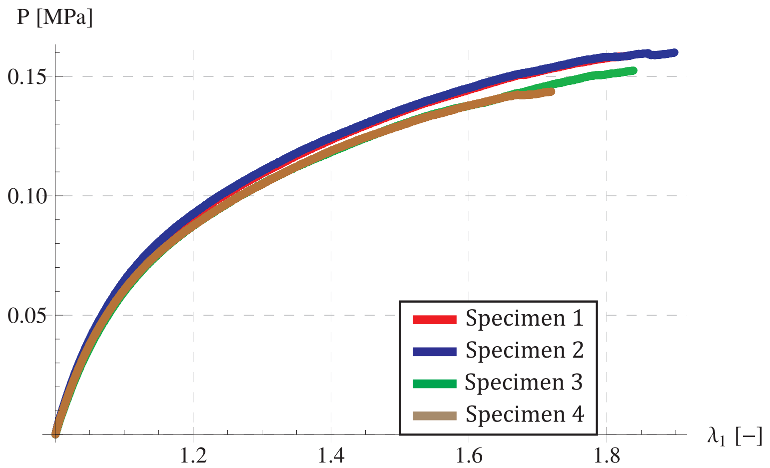

Figure 3.40: The stress-stretch curve of T-NMD-WL specimens

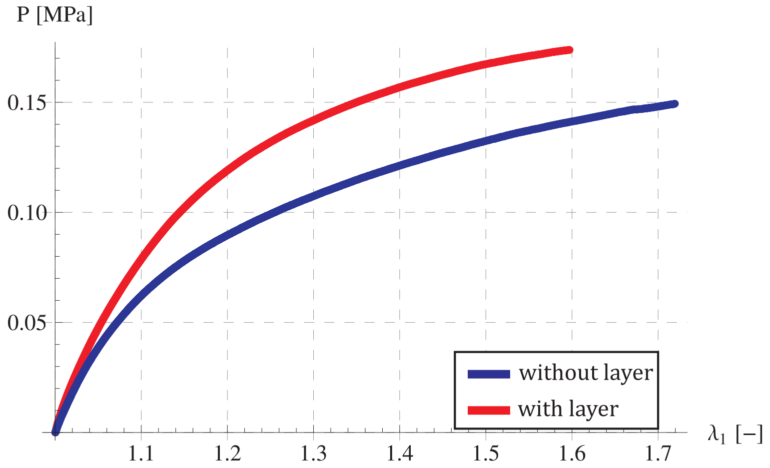

Figure 3.41: The comparison of T-NMD specimens' stress-stretch curve with and without layer

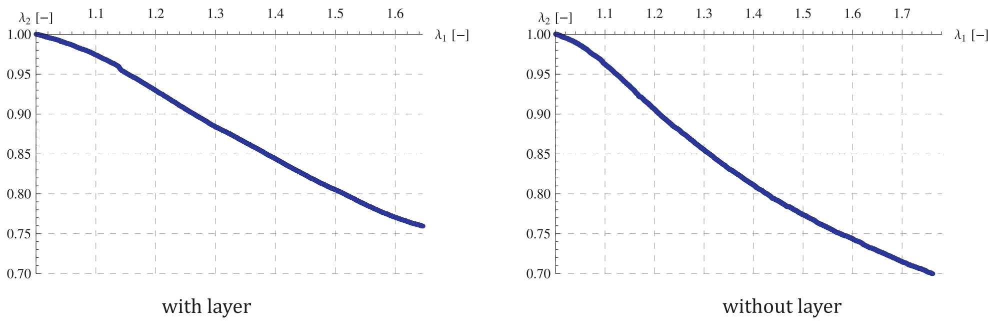

Figure 3.42: The relation between stretches (λ_1, λ_2) of T-NMD specimens with and without layer

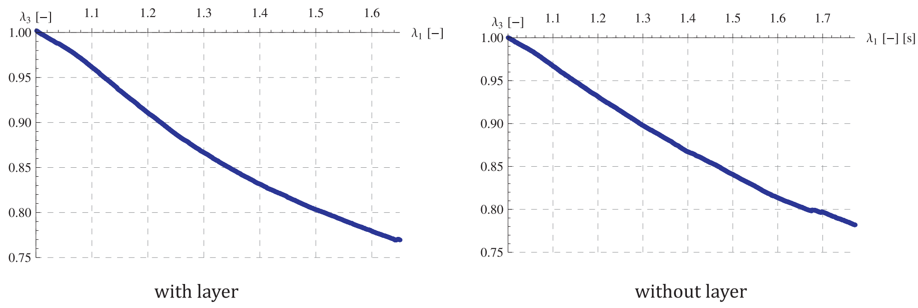

Figure 3.43: The relation between stretches (λ_1, λ_3) of T-NMD specimens with and without layer

3.3.4 Summary

As the tensile test represents, the skin layer makes the polymer foam more fragile: the initial elastic modulus (E^*) becomes higher, the tensile strength $(\sigma_{\max})$ increases, while the maximum stretch decreases. This effect can be explained again by the higher relative density of the skin layer because the elastic modulus and the formula describing the non-linear part is the function of relative density (Eqn. 2.15 and 2.23).

The tendencies of machine and non-machine direction tension are the same, because of the geometry of specimen is similar: the longitudinal direction is parallel with the skin layer.

3.4 Results of measurements

After the execution and evaluation of compression and tensile tests the full stress-stretch characteristic of the examined polyethylene foam sheet has been determined in machine and non-machine directions (Figures 3.44 and 3.45). As these figures show, the mechanical behaviour in case of uni-axial load corresponds with the theoretical description of closed-cell polymer foams in *Chapter 2*.

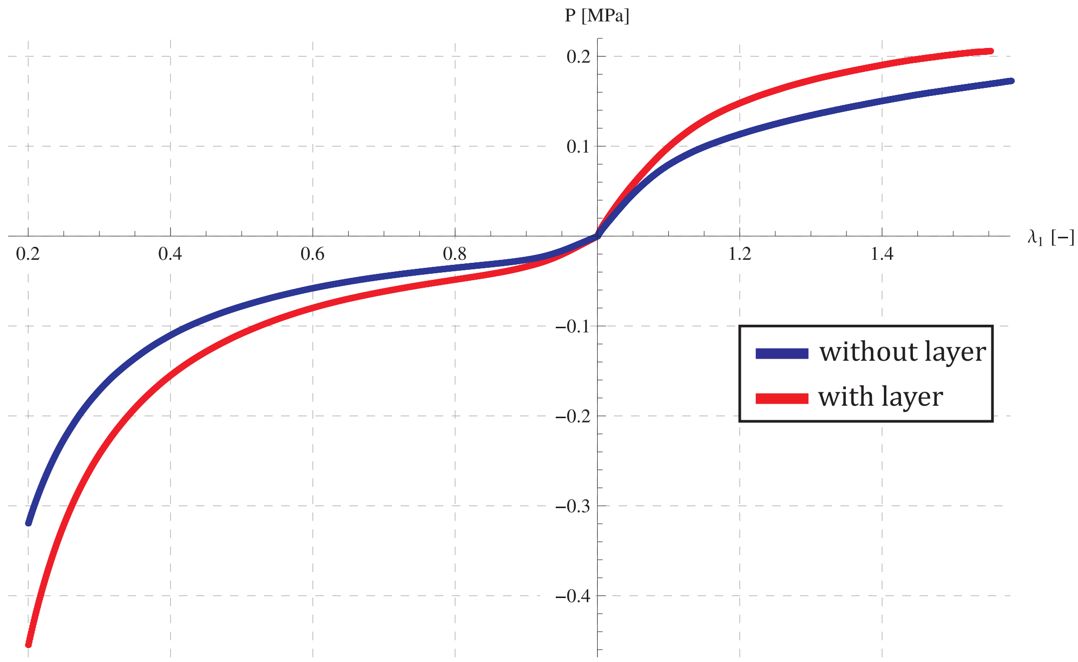

Figure 3.44: The stress-stretch characteristic of MD load with and without layer

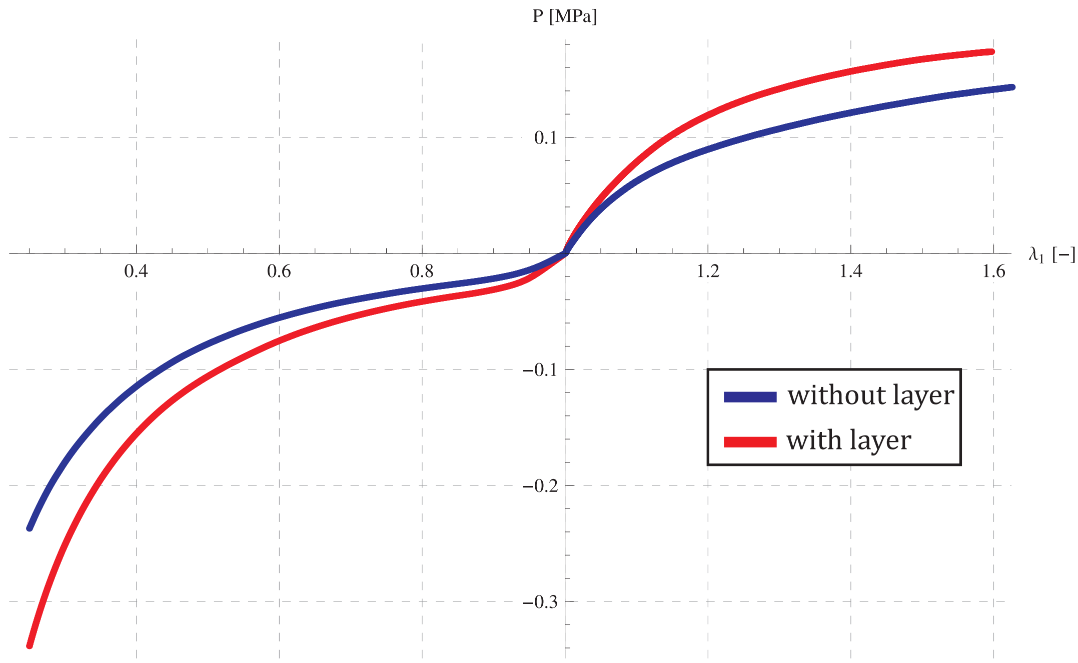

Figure 3.45: The stress-stretch characteristic of NMD load with and without layer

In case of layer-free specimens the stress values are always smaller, so the effect of skin layer can be established: it increases the strength of the foam, whereas in case of tension the maximum stretch decreases.

4

Hyperelastic model fitting

4.1 Introduction, theoretical summary

The following theoretical summary is based on the books of A. Bower (2010) [3], E. A. de Souza *et al.* (2008) [4] and I. Dorghi (2000) [5].

Hyperelastic theory is applied for nonlinear, elastic materials in case of large strains. The mechanical response of a typical polymer is temperature dependent: below the so-called T_g glass transition temperature it behaves as a glass. Above this temperature mechanical properties and mechanisms change and become rubbery: the moduli decreases, the stress is independent from strain history and rate, which is described in the hyperelastic constitutive laws. Moreover, this material model can be used for describing the mechanisms of polymer foams due to the similarity of mechanical properties described in *Chapter 2*.

All hyperelastic models are based on the scalar-valued function determining the stress-strain relation by defining the elastic potential of the body (per unit mass) as the function of the deformation gradient ($\boldsymbol{F}$) as

$$\psi = \psi(\boldsymbol{F}), \tag{4.1}$$

which ensures the elasticity of the material behaviour and enables the 1st Piola-Kichhoff stress tensor ($\boldsymbol{P}$) to be expressed by

$$\boldsymbol{P} = \rho_0 \frac{\partial \psi(\boldsymbol{F})}{\partial \boldsymbol{F}}, \tag{4.2}$$

where ρ_0 is the density in the reference consiguration. Simultaneously W, the elastic potential measured per unit volume can be defined as

$$W = \rho_0 \psi. \tag{4.3}$$

If it is expressed in the function of the right Cauchy-Green deformation tensor $\boldsymbol{C} = \boldsymbol{F}^T\boldsymbol{F}$, the 1st Piola-Kirchhoff stress tensor $\boldsymbol{P}$ becomes

$$\boldsymbol{P} = 2\boldsymbol{F}\frac{\partial W(\boldsymbol{C})}{\partial \boldsymbol{C}}. \tag{4.4}$$

Therefore, the other stress tensors can be expressed as the function of W, due to the connection between each other:

$$\boldsymbol{\tau}{=}2\boldsymbol{F}\frac{\partial W(\boldsymbol{C})}{\partial \boldsymbol{C}}\boldsymbol{F}^T, \tag{4.5}$$

$$\boldsymbol{\sigma}{=}\frac{2}{J}\boldsymbol{F}\frac{\partial W(\boldsymbol{C})}{\partial \boldsymbol{C}}\boldsymbol{F}^T, \tag{4.6}$$

where $\boldsymbol{\tau}$ is the Kirchhoff-stress and $\boldsymbol{\sigma}$ is the Cauchy-stress tensor and J is the determinant of $\boldsymbol{F}$. In case of elastically isotropic materials the elastic potential W depends on the scalar invariants (I_1, I_2 and I_3) of strain, which are constants, if the body is elastically homogenous. Therefore,

$$W = W(I_1, I_2, I_3) \tag{4.7}$$

where the principal invariants of $\boldsymbol{C}$ are determined by

$$I_1 = \mathrm{tr}[\boldsymbol{C}], \qquad I_2 = \frac{1}{2}(I_1^2 - \mathrm{tr}[\boldsymbol{C}^2], \qquad I_3 = \det \boldsymbol{C} = J^2. \tag{4.8}$$

The principal invariants of $\boldsymbol{C}$ can be expressed in the term of the principal stretches (λ_1, λ_2 and λ_3):

$$I_1 = \lambda_1^2 + \lambda_2^2 + \lambda_3^2, \qquad I_2 = (\lambda_1\lambda_2)^2 + (\lambda_1\lambda_3)^2 + (\lambda_2\lambda_3)^2, \qquad I_3 = (\lambda_1\lambda_2\lambda_3)^2. \tag{4.9}$$

Therefore, the elastic potential W in case of elastic homogenous isotropic materials can be given as

$$W = W(\lambda_1, \lambda_2, \lambda_3). \tag{4.10}$$

Using the chain-rule for derivation, the Kirchhoff stress tensor ($\boldsymbol{\tau}$) can be determined as:

$$\boldsymbol{\tau} = \sum_{a=1}^{3} \lambda_a \frac{\partial W}{\partial \lambda_a} \boldsymbol{n}^{(a)} \otimes \boldsymbol{n}^{(a)}, \tag{4.11}$$

where $\boldsymbol{n}^{(a)}$ are the unit eigenvectors of the left Cauchy-Green deformation tensor ($\boldsymbol{b}$).

The specific forms for elastic potencial W are based on experiments and contain the material properties, so the formula can be adjusted to the material being modelled. The most commonly used hyperelastic material model for polymer foam is the Ogden–Storåkers compressible hyperelastic model. It is included in the most widely-used commercial finite element softwares, such as ANSYS [2].

4.2 Ogden–Storåkers compressible hyperelastic model

4.2.1 Description of the model

The compressible hyperelastic model published by Storåkers in 1986 [11] describes the elastic potential of homogenous isotropic materials in the terms of the principal stretches (λ_i) as:

$$W = \sum_{i=1}^{N} \frac{2\mu_i}{\alpha_i^2} \left[\lambda_1^{\alpha_i} + \lambda_2^{\alpha_i} + \lambda_3^{\alpha_i} - 3 + \frac{1}{\beta_i} \left(J^{-\alpha_i \beta_i} - 1 \right) \right], \tag{4.12}$$

where μ_i, α_i and β_i are material properties, which should be determined via experimental investigations. The shear (μ_0) and bulk (K_0) moduli describing the initial behaviour of polymer foams (at small strains) can be computed by

$$\mu_0 = \sum_{i=1}^{N} \mu_i, \qquad K_0 = \sum_{i=1}^{N} 2\mu_i \left(\frac{1}{3} + \beta_i\right). \tag{4.13}$$

The material parameters β_i, which represents the degree of compressibility, is related to the Poisson's ration (ν) by

$$\beta_i = \frac{\nu_i}{1 - 2\nu_i}. \tag{4.14}$$

Towards a stable stress-free ground-state, the parameters have to fulfil the following requirements:

$$\sum_{i=1}^{N} \mu_i \alpha_i > 0 \qquad \textit{and} \qquad \beta_i > -\frac{1}{3}. \tag{4.15}$$

Now, according to Eqn. 4.11 the Kirchhoff stress is expressed as

$$\boldsymbol{\tau} = \sum_{A=1}^{3} \sum_{i=1}^{N} \frac{2\mu_i}{\alpha_i} \left(\lambda_A^{\alpha_i} - J^{-\alpha_i \beta_i}\right) \boldsymbol{n}^{(A)} \otimes \boldsymbol{n}^{(A)}, \tag{4.16}$$

where the principal Kirchhoff stresses are

$$\tau_A = \sum_{i=1}^{N} \frac{2\mu_i}{\alpha_i} \left(\lambda_A^{\alpha_i} - J^{-\alpha_i \beta_i}\right), \qquad (A = 1, 2, 3). \tag{4.17}$$

4.2.2 Solutions for homogenous deformations

In case of uniaxial tension and compression, like the measurements described in *Chapter 3*, the uniaxial extension is defined in a fixed Cartesian coordinate system by

$$x_1 = \lambda_1 X_1, \qquad x_2 = \lambda_2 X_2, \qquad x_3 = \lambda_3 X_3, \quad \text{and} \quad \lambda_2 = \lambda_3, \tag{4.18}$$

where direction 1 is the axis of deformation. Thus, the deformation gradient ($\boldsymbol{F}$) and the left Cauchy-Green deformation tensor ($\boldsymbol{b}$) are obtained as:

$$[\boldsymbol{F}] = \begin{bmatrix} \lambda_1 & 0 & 0 \\ 0 & \lambda_2 & 0 \\ 0 & 0 & \lambda_3 \end{bmatrix} \quad \text{and} \quad [\boldsymbol{b}] = \begin{bmatrix} \lambda_1^2 & 0 & 0 \\ 0 & \lambda_2^2 & 0 \\ 0 & 0 & \lambda_3^2 \end{bmatrix}. \tag{4.19}$$

Therefore, the principal invariants become

$$I_1 = \lambda_1^2 + \frac{2J}{\lambda_1}, \qquad I_2 = \frac{J}{\lambda_1}\left(2\lambda_1^2 + \frac{J}{\lambda_1}\right) \quad \text{and} \quad I_3 = \lambda_1^2 \lambda_2^4, \tag{4.20}$$

which means that the determinant of $\boldsymbol{F}$, will be $J = \lambda_1 \lambda_2^2$.

Now, according to (4.17) the principal Kirchhoff stresses can be determined as

$$\tau_1 = \sum_{i=1}^{N} \frac{2\mu_i}{\alpha_i} \left(\lambda_1^{\alpha_i} - \left(\lambda_1 \lambda_2^2\right)^{-\alpha_i \beta_i}\right), \tag{4.21}$$

$$\tau_2 = \tau_3 = 0 = \sum_{i=1}^{N} \frac{2\mu_i}{\alpha_i} \left(\lambda_2^{\alpha_i} - \left(\lambda_1 \lambda_2^2 \right)^{-\alpha_i \beta_i} \right). \tag{4.22}$$

In the case, when $N = 1$ only 3 model parameters are required which are denoted as (α, β and μ). The principal stresses reduce to

$$\tau_1 = \frac{2\mu}{\alpha} \left(\lambda_1^{\alpha} - \left(\lambda_1 \lambda_2^2 \right)^{-\alpha\beta} \right), \tag{4.23}$$

$$\tau_2 = \tau_3 = 0 = \frac{2\mu}{\alpha} \left(\lambda_2^{\alpha} - \left(\lambda_1 \lambda_2^2 \right)^{-\alpha\beta} \right) \tag{4.24}$$

From the second equation the relation between λ_1 and λ_2 can be expressed as

$$\lambda_2 = \lambda_1^{\frac{-\beta}{1+2\beta}}, \tag{4.25}$$

which indicates, that by measuring the stretch in the perpendicular direction material parameter β can be determined. Moreover using the formula above (4.25) the perpendicular stretches can be eliminated. So, the principal Kirchhoff (τ_1), Cauchy (σ_1) and 1st Piola-Krichhoff (P_1) stresses (in the axis of deformation) become

$$\tau_1 = \frac{2\mu}{\alpha} (1 - \lambda_1^{-\alpha \frac{1+3\beta}{1+2\beta}}) \lambda_1^{\alpha}, \tag{4.26}$$

$$\sigma_1 = \frac{\tau_1}{J} = \frac{2\mu}{\alpha} (1 - \lambda_1^{-\alpha \frac{1+3\beta}{1+2\beta}}) \lambda_1^{\alpha - \frac{1}{1+2\beta}}, \tag{4.27}$$

$$P_1 = \frac{\tau_1}{\lambda_1} = \frac{2\mu}{\alpha} (1 - \lambda_1^{-\alpha \frac{1+3\beta}{1+2\beta}}) \lambda_1^{\alpha - 1}. \tag{4.28}$$

From stresses, the load (F_1) could be determined as

$$F_1 = P_1 A_0 = \sigma_1 A = \frac{2\mu}{\alpha} A_0 (1 - \lambda_1^{-\alpha \frac{1+3\beta}{1+2\beta}}) \lambda_1^{\alpha - 1}, \tag{4.29}$$

where A_0 is the initial and A is the actual area of the cross-section ($A = \lambda_2^2 A_0$).

4.3 Determination of material parameters

4.3.1 Introduction

After having the stress-stretch ($P_1 - \lambda_1$) characteristic of all type of specimens and the proper hyperelastic material model, the parameters of the model should have been determined adequately in order to describe the behaviour of our polyethylene foam by using the hyperelastic model. As Eqn. 4.21 shows, originally the material model expresses the Kirchhoff-stress (τ) in function of the stretches ($\lambda_1, \lambda_2, \lambda_3$). However, in our case as the result of the measurements the 1st Piola-Kirchhoff stress (P) was determined in the term of the stretches. By using the relation between the Kirchhoff and the 1st Piola-Kirchhoff stresses ($\lambda_1 P_1 = \tau_1$) the formula, used for model fitting, becomes

$$P_1 = \sum_{i=1}^{N} \frac{1}{\lambda_1} \frac{2\mu_i}{\alpha_i} \left(\lambda_1^{\alpha_i} - \left(\lambda_1 \lambda_2^2 \right)^{-\alpha_i \beta_i} \right). \tag{4.30}$$

During our test, the load was uniaxial, thus the cross-direction stretches considered to be equal ($\lambda_2 = \lambda_3$), and simultaneously the stresses in these directions (P_2, P_3) should be zero:

$$P_2 = P_3 = 0 = \sum_{i=1}^{N} \frac{2\mu_i}{\alpha_i} \left(\lambda_2^{\alpha_i} - \left(\lambda_1 \lambda_2^2 \right)^{-\alpha_i \beta_i} \right). \tag{4.31}$$

4.3.2 Relation of stretches

In the material model, we used, the cross-direction stretches are equal, whereas during our measurements the cross-direction stretches were different. Therefore an equivalent cross-direction stretch was should be determined. According to the articles of W. H. El-Ratal *et al.* [6] and J. G. Murphy *et al.* [16], the relationship between the longitudinal and the cross-direction stresses can be approximated as

$$\lambda_2 = \lambda_1^{-\nu_2} \quad and \quad \lambda_3 = \lambda_1^{-\nu_3}, \tag{4.32}$$

where ν_2 and ν_3 has the same significance as the Poisson's ratio of linear elasticity. This model can be used for compression and tension as well. So firstly in case of all tests, when the cross-direction stretches were measured by video, the ν_2 or ν_3 exponents were determined using the "FindFit" [17] built-in curve fitting algorithm of *Wolfram Mathematica* [18] on the longitudnial and cross-direction stretch (see in the `Appendix`). The process of curve fitting is illustrated in Figure 4.1 and the results are listed in Table 4.1.

Specimen	ν_2	ν_3	Specimen	ν_2	ν_3
C-T-1	0.074994	-	T-MD-1	0.491597	-
C-T-2	0.036279	-	T-MD-2	0.531452	-
C-T-3	0.041896	-	T-MD-3	-	0.586345
C-T-4	0.048417	-	T-MD-4	-	0.600846
C-T-WL-2	0.04116	-	T-MD-WL-1	0.708484	-
C-T-WL-3	0.068218	-	T-MD-WL-2	0.690772	-
C-T-WL-4	0.032393	-	T-MD-WL-3	-	0.545735
C-MD-1	0.091375	-	T-MD-WL-4	-	0.5521658
C-MD-2	0.10193	-	T-NMD-1	-	0.534716
C-MD-3	-	0.051712	T-NMD-2	-	0.546272
C-MD-4	-	0.046257	T-NMD-3	0.447526	-
C-MD-WL-1	0.089747	-	T-NMD-4	0.51253	-
C-MD-WL-2	0.108854	-	T-NMD-WL-1	-	0.468317
C-MD-WL-3	-	0.032119	T-NMD-WL-2	-	0.466648
C-MD-WL-4	-	0.065945	T-NMD-WL-3	0.620886	-
C-NMD-2	0.085285	-	T-NMD-WL-4	0.654186	-
C-NMD-3	-	0.0241735			
C-NMD-WL-2	0.015436	-			
C-NMD-WL-3	-	0.021923			

Table 4.1: The calculated ν_2 and ν_3 values

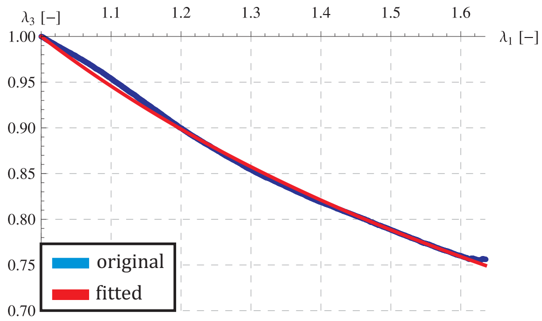

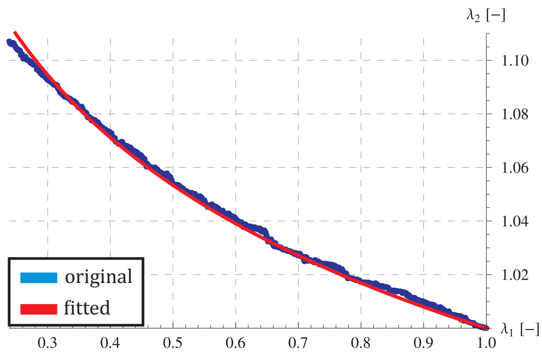

Figure 4.1: The curve fitting on the λ_1 - $\lambda_{2,3}$ characteristics in case of tension and compression

From the results of the curve fitting, both exponents (ν_2, ν_3) were determined in all type of specimens as the mean values of the curve fitting. In case of thickness direction compression (C-T), because of the geometry, the cross-direction stretches were presumed to be equal, so in this case $\nu_2 = \nu_3$.

Specimen type	ν_2	ν_3
C-T	0.050396	0.050396
C-T-WL	0.047257	0.047257
C-MD	0.096652	0.048984
C-MD-WL	0.099301	0.049032
C-NMD	0.085285	0.024174
C-NMD-WL	0.015436	0.021923
T-MD	0.511525	0.593596
T-MD-WL	0.699628	0.5457356
T-NMD	0.480028	0.540494
T-NMD-WL	0.637536	0.447483

Table 4.2: The resultant ν_2 and ν_3 values of each specimen type

From these resultant (ν_2, ν_3) exponents the equivalent cross-direction stretch can be expresses as

$$\bar{\lambda}_2 = \lambda_1^{-\frac{\nu_2+\nu_3}{2}}, \tag{4.33}$$

which has the same effect as the two different cross-direction stresses measured during the tests.

4.3.3 Correction factor

In case of tensile test, the stretch of the gauge length, shown as L_0 in Figure 3.28, is not equal to the stretch measured by the displacement of the cross-head. Therefore a correction factor (c) should be determined to receive the proper stretch (λ_1) values of the tensile test calculated from the measured stretch (λ_{MES}). The initial stretch should remain 1, therefore the proper stretch becomes:

$$\lambda_1 = c \cdot \lambda_{MES} - (c - 1). \tag{4.34}$$

As written in *Chapter 3*, markers were placed on the surface of some specimens. From the video processed data the relation of the crosshead stretch (λ_{CH}) and by the marker tracking (λ_M) was determined. This connection was described by covariant coefficient of the linear regression fitting

$$\lambda_M = c\lambda_{CH} + \beta, \tag{4.35}$$

where c is the correction factor and β is the so-called error term of the linear regression. The results of the regression calculation are presented in the following table (Table 4.3).

Specimen	c
T-MD-01	1.05877
T-MD-02	1.0399
T-NMD-01	1.06049
T-NMD-02	1.0924

Table 4.3: The calculated correction factor (c) values

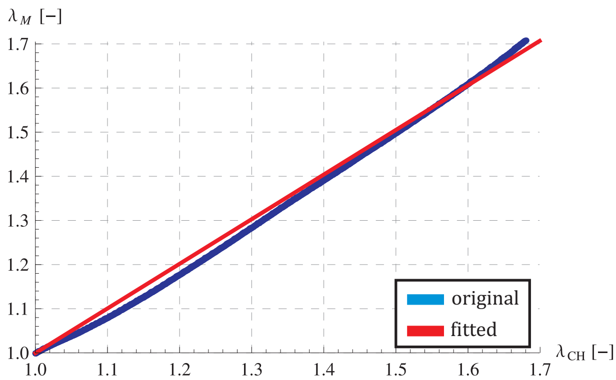

Figure 4.2: The curve fitting on the λ_{CH}-λ_M characteristics

The resultant correction factor used for adjusting the stretches was given as the mean of the correction factors in Table 4.3.

$$c = \frac{1}{4}\sum_{i=1}^{4} c_i = 1.06289. \tag{4.36}$$

It should be noted, that very small difference can be observed between the stretches measured by the crosshead and the markers.

4.3.4 Procedure of fitting

The hyperelastic model fitting was performed in *Wolfram Mathematica* [18] by using two built-in curve fitting algorithms: "*Findfit*" [17] and "*NMinimize*"[19], where the latter one is a numerical procedure for contrained minimisation (see in the `Appendix`). The *FindFit* [17] algorithm is easier to use, it finds the coefficients by using the least-square method with good accuracy to describe only the $(P_1 - \lambda_1)$ characteristic. But the cross-directional stress (P_2) cannot be set up zero, so we receive cross-directional stresses as well, thus the error of curve fitting becomes significant.

When using the *NMinimize* [19] algorithm, an error function should be defined. The error was determined according to the least square method used for the longitudinal direction and the cross-direction stresses as well:

$$e = \sum_{i=1}^{N} [(P_{1i} - P_{1i\_fitted})^2 + P^2_{2ifitted}] \tag{4.37}$$

where N is the number of measurement points.

The *NMinimize* [19] algorithm gives the coefficients of the material model by finding the minimum of the error function numerically. As a method for searching the minimum the "*Simulated Annealing*" stochastic function minimizer was used. This algorithm gives better accuracy and the cross-direction stress was taken into consideration as well.

Initially, I used a first-order Ogden–Storåkers model containing 3 material parameters (α, β, μ), but as the result shows, its accuracy is not satisfactory. Therefore a second-order model was fitted, in this case 6 material parameters $(\alpha_1, \beta_1, \mu_1, \alpha_2, \beta_2, \mu_2)$ were calculated. Both models (first- and second-order) was fitted by both algorithms so finally we received four series of parameters.

In all cases the maximum of the cross-direction stress and the error value (computed by the least square method) were given representing the quality of the model fitting.

4.3.5 Results

After the process of the curve fitting, the received parameters were compared by computing the error of the fitted model using the formula (Eqn 4.37) mentioned above. After analysing the errors, the series of parameters having the smallest error were chosen as the best fitting model. The resultant longitudinal and cross-direction stresses (P_1, P_2) and the measured longitudinal stress are displayed in the corresponding figure. In all cases a second-order model found by "Nminimize" method had the smallest error, therefore this was chosen the best fitted model.

4.3.5.1 Compression - Machine direction

With layer

Type of fitting	α_1	β_1	μ_1	α_2	β_2	μ_2
"FindFit" 1st order	0.2414	13.299	0.0504	-	-	-
"NMinimize" 1st order	0.1422	7.622	0.0851	-	-	-
"FindFit" 2nd order	0.24136	13.488	0.05126	$-2.93 \cdot 10^{-7}$	-6.3179	-0.231929
"NMinimize" 2nd order	0.08043	7.62203	0.0850611	0.061728	7.62203	0.0850611

Table 4.4: The parameters of the hyperelastic model in case of C-MD specimens

Type of fitting	Error (e)
"FindFit" 1st order	8.32012
"NMinimize" 1st order	0.00966
"FindFit" 2nd order	8.25844
"NMinimize" 2nd order	0.00965

Table 4.5: The error of hyperelastic model in case of C-MD specimens

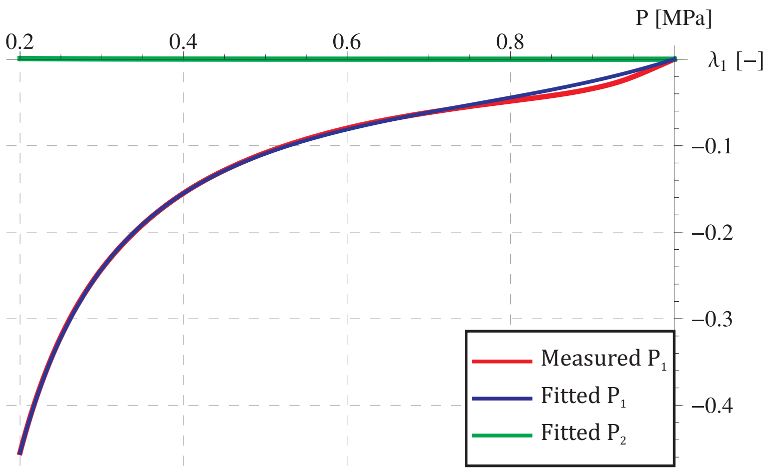

Figure 4.3: The stresses of the best fitted model in case of C-MD specimens

Without layer

Type of fitting	α_1	β_1	μ_1	α_2	β_2	μ_2
"FindFit" 1st order	0.20437	15.4529	0.04168	-	-	-
"NMinimize" 1st order	0.09731	7.1161	0.08679	-	-	-
"FindFit" 2nd order	0.059752	3.0685	0.08811	$2.75 \cdot 10^{-7}$	2.5285	3.0897
"NMinimize" 2nd order	0.082097	7.1161	0.08679	0.01521	7.1161	0.08679

Table 4.6: The parameters of the hyperelastic model in case of C-MD-WL specimens

Type of fitting	Error (e)
"FindFit" 1st order	12.8672
"NMinimize" 1st order	0.00911
"FindFit" 2nd order	0.06976
"NMinimize" 2nd order	0.00907

Table 4.7: The error of hyperelastic model in case of C-MD-WL specimens

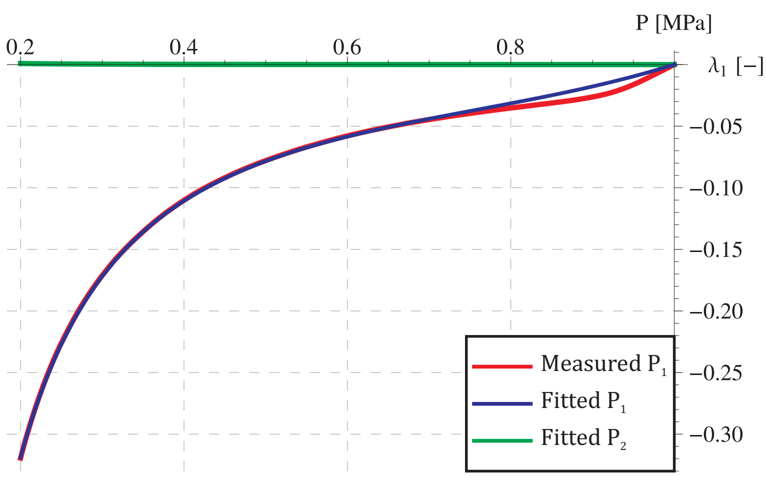

Figure 4.4: The stresses of the best fitted model in case of C-MD-WL specimens

4.3.5.2 Compression - Non-machine direction

With layer

Type of fitting	α_1	β_1	μ_1	α_2	β_2	μ_2
"FindFit" 1st order	0.224412	14.2916	0.05701	-	-	-
"NMinimize" 1st order	0.208059	13.1954	0.061448	-	-	-
"FindFit" 2nd order	0.001888	0.01946	11.204	0.312249	24.5998	-0.00956
"NMinimize" 2nd order	0.18805	13.4922	0.044217	0.0062773	1.62681	0.63769

Table 4.8: The parameters of the hyperelastic model in case of C-NMD specimens

Type of fitting	Error (e)
"FindFit" 1st order	0.053197
"NMinimize" 1st order	0.003987
"FindFit" 2nd order	5.71405
"NMinimize" 2nd order	0.002945

Table 4.9: The error of hyperelastic model in case of C-NMD specimens

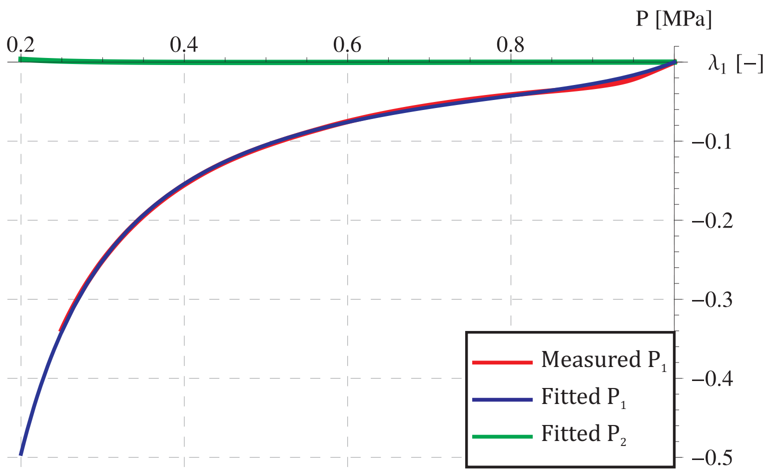

Figure 4.5: The stresses of the best fitted model in case of C-NMD specimens

Without layer

Type of fitting	α_1	β_1	μ_1	α_2	β_2	μ_2
"FindFit" 1st order	0.12073	9.8381	0.06891	-	-	-
"NMinimize" 1st order	0.43623	38.0723	0.01943	-	-	-
"FindFit" 2nd order	0.21856	16.8193	-0.32491	0.03899	2.3284	0.18989
"NMinimize" 2nd order	0.19764	23.4786	0.01925	0.01313	0.42027	0.02328

Table 4.10: The parameters of the hyperelastic model in case of C-NMD-WL specimens

Type of fitting	Error (e)
"FindFit" 1st order	0.974634
"NMinimize" 1st order	0.011376
"FindFit" 2nd order	8.93604
"NMinimize" 2nd order	$8.83{\cdot}10^{-5}$

Table 4.11: The error of hyperelastic model in case of C-NMD-WL specimens

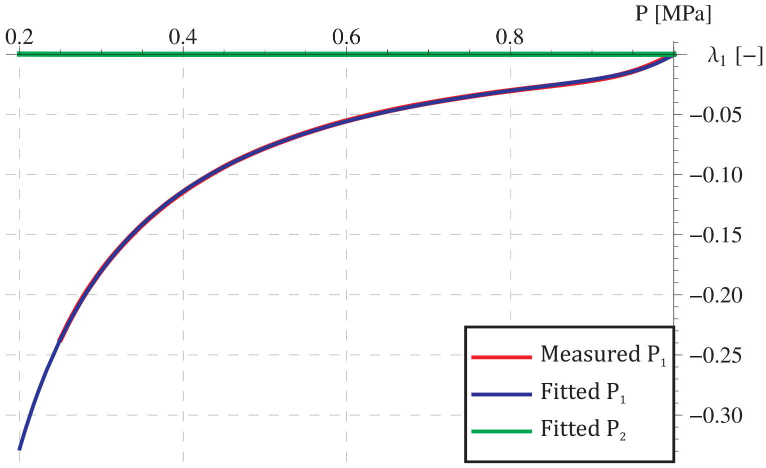

Figure 4.6: The stresses of the best fitted model in case of C-NMD-WL specimen

4.3.5.3 Compression - Thickness

With layer

Type of fitting	α_1	β_1	μ_1	α_2	β_2	μ_2
"FindFit" 1st order	0.11416	5.89458	0.09829	-	-	-
"NMinimize" 1st order	0.20427	11.2619	0.05612	-	-	-
"FindFit" 2nd order	0.17172	14.4548	-0.00419	0.01776	0.70022	0.48175
"NMinimize" 2nd order	0.0204	1.42564	0.411557	0.13479	11.5345	0.00308

Table 4.12: The parameters of the hyperelastic model in case of C-T specimens

Type of fitting	Error (e)
"FindFit" 1st order	1.09466
"NMinimize" 1st order	0.015663
"FindFit" 2nd order	0.87387
"NMinimize" 2nd order	0.00113

Table 4.13: The error of hyperelastic model in case of C-T specimens

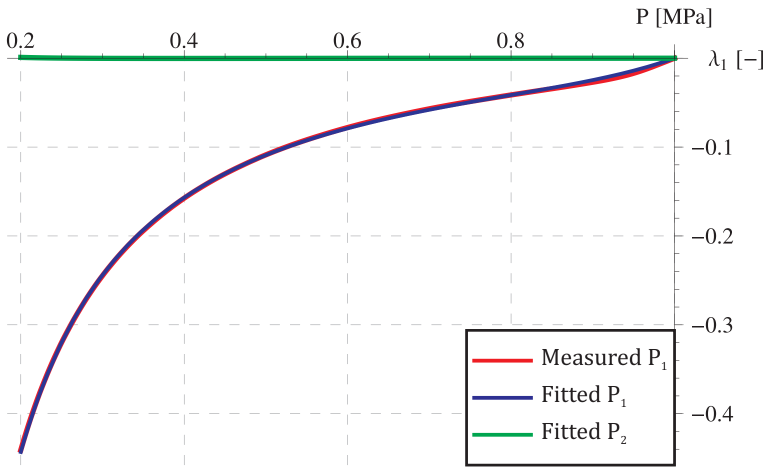

Figure 4.7: The stresses of the best fitted model in case of C-T specimen

Without layer

Type of fitting	α_1	β_1	μ_1	α_2	β_2	μ_2
"FindFit" 1st order	0.09799	7.7107	0.06891	-	-	-
"NMinimize" 1st order	0.18141	14.5121	0.01943	-	-	-
"FindFit" 2nd order	$-9.95 \cdot 10^{-10}$	2.36576	2.6999	0.113972	9.43545	0.08338
"NMinimize" 2nd order	0.12674	13.1997	0.052	0.008779	0.44775	0.05796

Table 4.14: The parameters of the hyperelastic model in case of C-T-WL specimens

Type of fitting	Error (e)
"FindFit" 1st order	1.16046
"NMinimize" 1st order	0.006832
"FindFit" 2nd order	0.959441
"NMinimize" 2nd order	0.00011

Table 4.15: The error of hyperelastic model in case of C-T-WL specimens

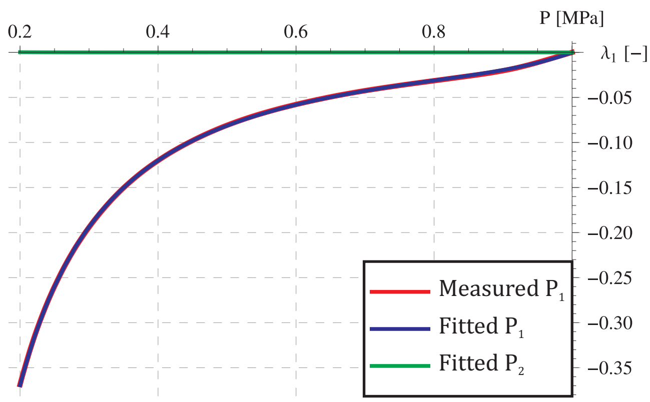

Figure 4.8: The stresses of the best fitted model in case of C-T-WL specimen

4.3.5.4 Tension - Machine direction

With layer

Type of fitting	α_1	β_1	μ_1	α_2	β_2	μ_2
"FindFit" 1st order	0.39778	$1.88 \cdot 10^{-9}$	0.01651	-	-	-
"NMinimize" 1st order	0.20357	3.0034	-0.3333	-	-	-
"FindFit" 2nd order	25.7025	0.06213	7.22495	-7.06532	0.22602	1.92779
"NMinimize" 2nd order	-303.757	2.57162	-0.32843	304.061	2.56905	-0.3333

Table 4.16: The parameters of the hyperelastic model in case of T-MD specimens

Type of fitting	Error (e)
"FindFit" 1st order	12.0645
"NMinimize" 1st order	4.0006
"FindFit" 2nd order	194156
"NMinimize" 2nd order	0.106819

Table 4.17: The error of hyperelastic model in case of T-MD specimens

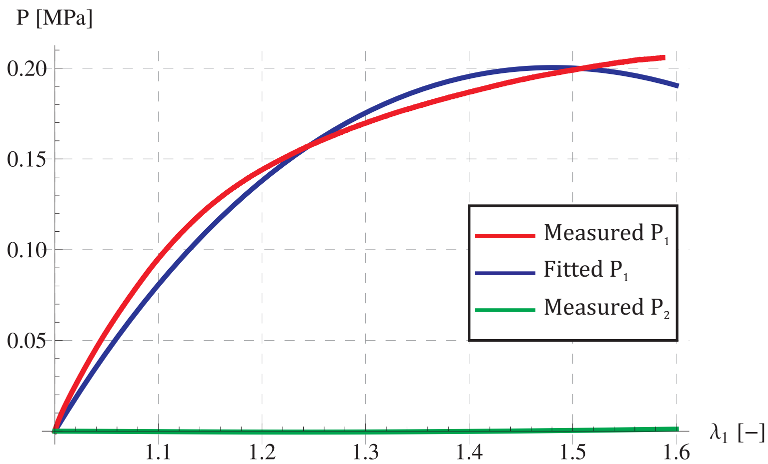

Figure 4.9: The stresses of the best fitted model in case of T-MD specimen

Without layer

Type of fitting	α_1	β_1	μ_1	α_2	β_2	μ_2
"FindFit" 1st order	0.305248	$3.21 \cdot 10^{-10}$	0.008438	-	-	-
"NMinimize" 1st order	0.149396	2.64505	-0.3333	-	-	-
"FindFit" 2nd order	6.02105	0.709662	3.97192	0.450272	-9.48963	0.231519
"NMinimize" 2nd order	0.33151	-1.10958	-0.3333	-0.11976	-4.74863	6.89511

Table 4.18: The parameters of the hyperelastic model in case of T-MD-WL specimens

Type of fitting	Error (e)
"FindFit" 1st order	11.2889
"NMinimize" 1st order	2.53203
"FindFit" 2nd order	40410.7
"NMinimize" 2nd order	0.051206

Table 4.19: The error of hyperelastic model in case of T-MD-WL specimens

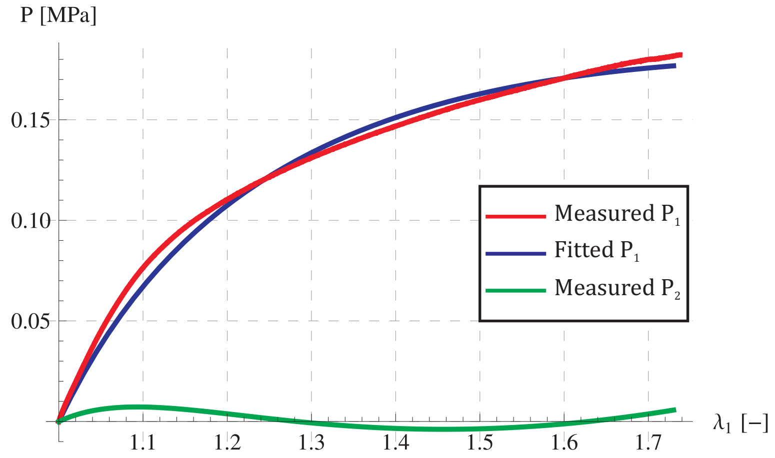

Figure 4.10: The stresses of the best fitted model in case of T-MD-WL specimen

4.3.5.5 Tension - Non-machine direction

With layer

Type of fitting	α_1	β_1	μ_1	α_2	β_2	μ_2
"FindFit" 1st order	0.321218	-2.14·10^{-9}	0.09431	-	-	-
"NMinimize" 1st order	0.164993	2.87478	-0.3333	-	-	-
"FindFit" 2nd order	8.14481	0.518944	13.4023	-5.47018	0.77268	-0.24126
"NMinimize" 2nd order	-0.33033	-5.74166	24.722	0.591589	-3.20599	-0.3333

Table 4.20: The parameters of the hyperelastic model in case of T-NMD specimens

Type of fitting	Error (e)
"FindFit" 1st order	7.31049
"NMinimize" 1st order	2.78752
"FindFit" 2nd order	3534.39
"NMinimize" 2nd order	0.02301

Table 4.21: The error of hyperelastic model in case of T-NMD specimens

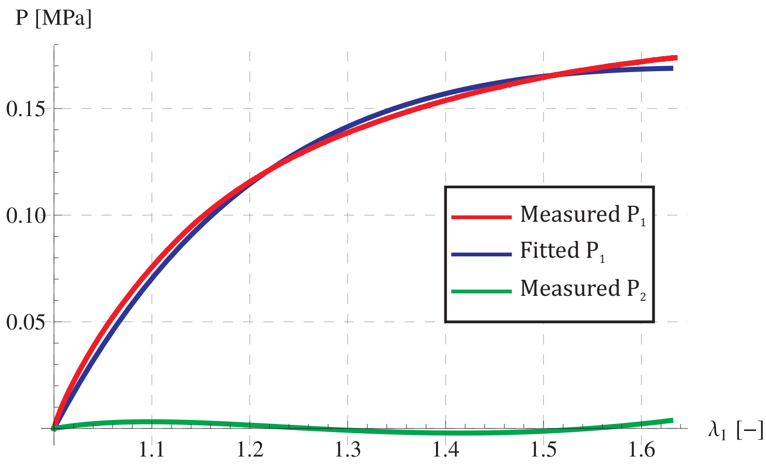

Figure 4.11: The stresses of the best fitted model in case of T-NMD specimen

Without layer

Type of fitting	α_1	β_1	μ_1	α_2	β_2	μ_2
"FindFit" 1st order	0.245056	$1.36{\cdot}10^{-8}$	0.02327	-	-	-
"NMinimize" 1st order	0.12138	2.62107	-0.3333	-	-	-
"FindFit" 2nd order	-0.83557	-27.5565	0.03431	8.61713	-26.7205	-0.20788
"NMinimize" 2nd order	0.41706	-2.26412	-0.3333	-0.23318	-4.04962	5.39818

Table 4.22: The parameters of the hyperelastic model in case of T-NMD-WL specimens

Type of fitting	Error (e)
"FindFit" 1st order	5.73196
"NMinimize" 1st order	1.70619
"FindFit" 2nd order	$9.17{\cdot}10^{6}$
"NMinimize" 2nd order	0.03686

Table 4.23: The error of hyperelastic model in case of T-NMD-WL specimens

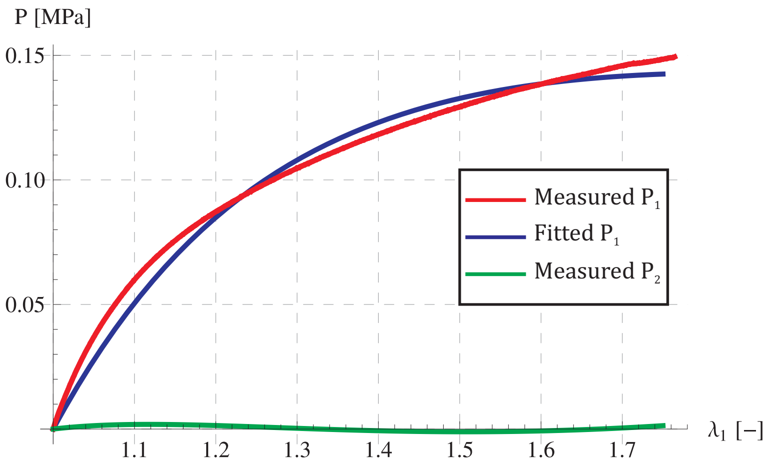

Figure 4.12: The stresses of the best fitted model in case of T-NMD-WL specimen

4.3.6 Summary

As the results show, in all cases the best fitted model was received by using a second-order "NMinimize" method. In this method in contrast to the "FindFit" method the conditions for the cross-direction stresses were taken into consideration, thus the total error of the fitting become less by orders.

In case of compression, the model could be fitted with great accuracy, difference can be observed only at the first linearly elastic regime of the stress-strain curve ($P_1 - \lambda_1$). The cross-directional stress (P_2) is approximately zero in the margin of acceptable error. Similarly, the cross-directional stretch (λ_2) characteristic is described with great accuracy by the fitted model.

When the load is tensile, the error of the model fitting increases. The main reason is that the original material model was designed for describing material behaviours where the longitudinal stress (P_1) should increase progressively. Although in case of our polyethylene foam the characteristic is rather digressive. Therefore, the accuracy of the material model fitting becomes worse and the values of the parameters are negative in some cases. However, the accuracy of model fitting describes the material behaviour with adequate accuracy for numerical simulations. The cross-directional stress (P_2) is again close to zero, although it became oscillating thanks to the deviation of the material parameters. Similarly the cross-direction stretch characteristic ($\lambda_1 - \lambda_2$) shows only little error comparing to the measured data.

In spite of the numerical errors of curve fitting occurring especially in case of the tensile test, the Ogden–Storåkers hyperelastic material model is suitable for describing the mechanical behaviour of our polymer foam.

5
Finite element analysis

5.1 Introduction

As the result of *Chapter 4* shows, a possible hyperelastic material model was fitted to the results of each type of specimens by finding the optimum of material parameters required to describe the behaviour of our specimens. Therefore we have the opportunity of applying the material model in a finite element program to simulate the experiments and to compare the results.

The commercial finite element simulation program, *ANSYS Mechanical 13.0* [2] was used, which has the Ogden–Storåkers hyperelastic material model built-in. Although in ANSYS [2], according to the Theoretical Reference [1], the definition for W (the elastic potential measured per unit volume) is

$$W = \sum_{i=1}^{N} \frac{\mu_{i\_ANSYS}}{\alpha_i} \left[\lambda_1^{\alpha_i} + \lambda_2^{\alpha_i} + \lambda_3^{\alpha_i} - 3 + \frac{1}{\beta_i} \left(J^{-\alpha_i \beta_i} - 1 \right) \right], \tag{5.1}$$

which shows a bit difference from the elastic potential determined orginially in Eqn. 4.12. This difference is caused by the definition of material parameters μ_i. After reducing the equations the material parameters μ_{i_ANSYS} in ANSYS [2] can be expressed as

$$\mu_{i\_ANSYS} = 2\frac{\mu_i}{\alpha_i}. \tag{5.2}$$

Therefore, the material parameters of the fitted model adequate for the simulation in ANSYS [2] are listed in the following Table (5.1).

Type of specimen	α_1	β_1	μ_1	α_2	β_2	μ_2
C-MD	0.0211	7.62203	0.0850611	0.0161972	7.62203	0.0850611
C-MD-WL	0.02307	7.11611	0.0867973	0.004276	7.11611	0.0867973
C-NMD	0.02787	13.4922	0.044218	0.007717	1.62861	0.63769
C-NMD-WL	0.016836	23.4786	0.01924	0.062506	0.420277	0.02328
C-T	0.028621	1.42564	0.411557	0.023371	11.5345	0.003079
C-T-WL	0.019204	13.1997	0.05201	0.039215	0.44776	0.05796
T-MD	-236.2378	2.57162	-0.32843	236.71085	2.56905	-0.3333
T-MD-WL	-0.59754	-1.10958	-0.3333	0.050441	-4.74863	6.89511
T-NMD	0.11506	-5.74166	24.722	-0.36905231	-3.20599	-0.3333
T-NMD-WL	-0.36841	-2.26412	-0.3333	0.115159	-4.04962	5.39818

Table 5.1: The proper parameters of the hyperelastic model for Ansys

These material parameters describe the same material behaviour as the fitted curves in *Chapter 4*. The aim of the finite element analysis is to compare the measured and the numerical results of each type of specimens, in the purpose of the verification of the fitted material model.

5.2 Simulation of the experiments

The finite element analysis of the measurement was a 3D structural analysis. The element type was chosen to be an 8-node brick (8-node 185), which has the possibility of modelling hyperelasticity. As material model the Ogden Compressible Foam model was chosen with the parameters listed above.

In case of all measurements the load was uniaxial and the stresses were considered to be homogenous, so the same geometry was built for all simulations. The model is an eighth part cubic model which width is 1 mm. On the symmetry sides zero displacement should have been applied, in order to simulate the deformation properly. The geometrical model is shown in Figure 5.1, with the coordinate system used in ANSYS.

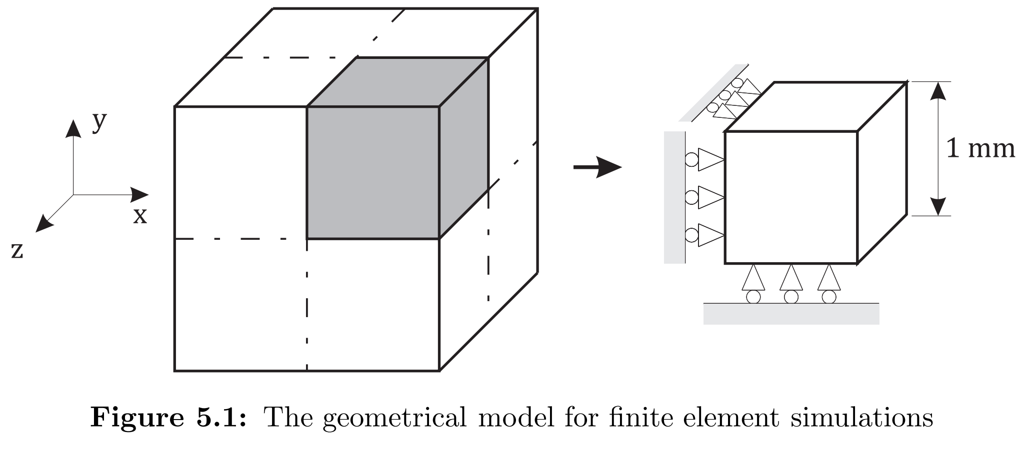

Figure 5.1: The geometrical model for finite element simulations

Because of the same considerations a one-element mesh was created, which contains the whole geometry. The deformation was modelled as a constant displacement. In case of compression as displacement -0.8 mm, in case of tension 0.55 mm was chosen accordingly to the results of the measurements.

This displacement was executed in the first step of the simulation, but our goal is to receive the stress-stretch curve, so sub-steps were required. During the simulations 500 sub-steps were used, which results the stress-stretch curve approximately with adequate sampling rate for the comparison with the measured data. Additionally large static displacement was permitted, which models the effect of large strains.

5.3 Results of simulations

When the simulation was complete, the following data were received in every sub-step: longitudinal displacement (ΔL_1), longitudinal stress (P_1), cross-direction displacement (ΔL_2) and cross-direction stress (P_2). These results were post-processed in *Wolfram Mathematica* [18], and we received the stress-strain diagram, showing the measured and the numerical longitudinal (P_1) and the numerical cross-direction (P_2) stresses (see in the `Appendix`). Simultaneously the cross-direction stretch (λ_2) was determined in the terms of the longitudinal stretch (λ_1) in case of the measurements and the finite element analysis as well.

5.3.1 Compression - Machine direction

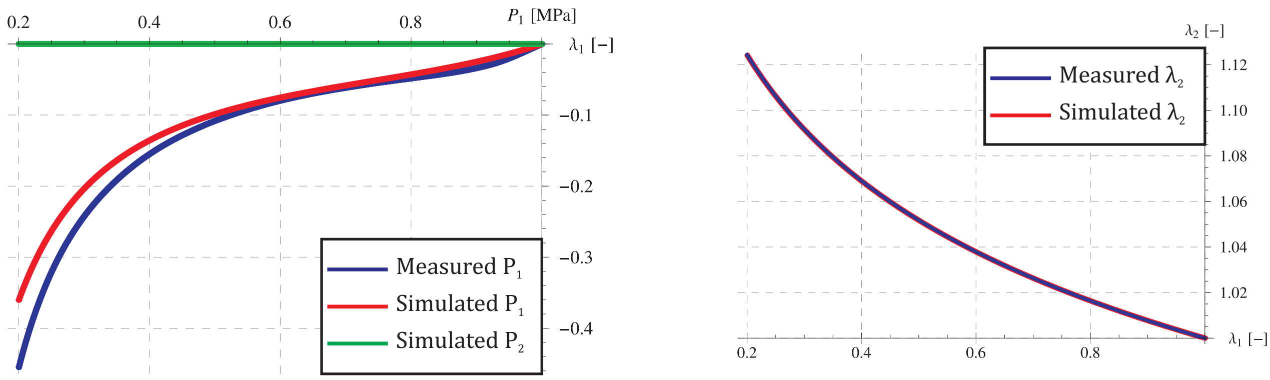

Stress-stretch curves

Longitudinal stretch characteristic

Figure 5.2: The results of C-MD simulations

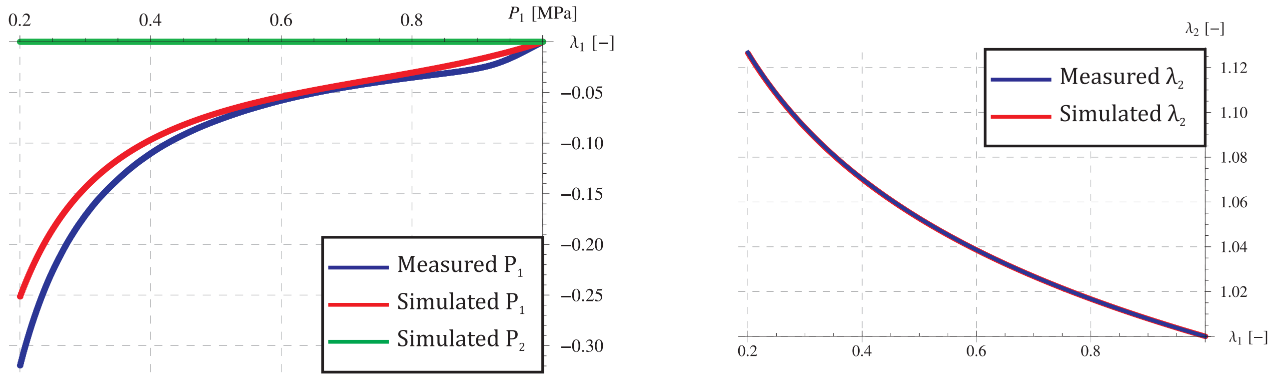

Stress-stretch curves

Longitudinal stretch characteristic

Figure 5.3: The results of C-MD-WL simulations

5.3.2 Compression - Non-machine direction

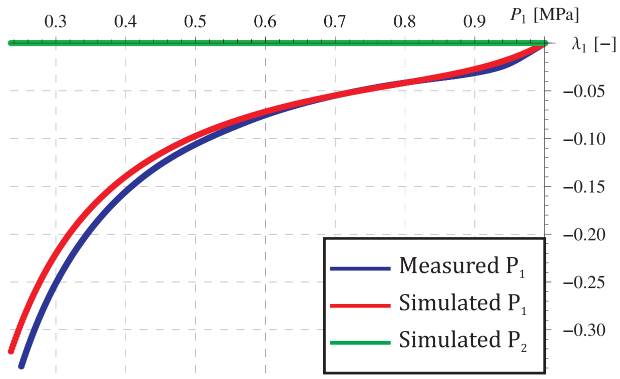

Stress-stretch curves

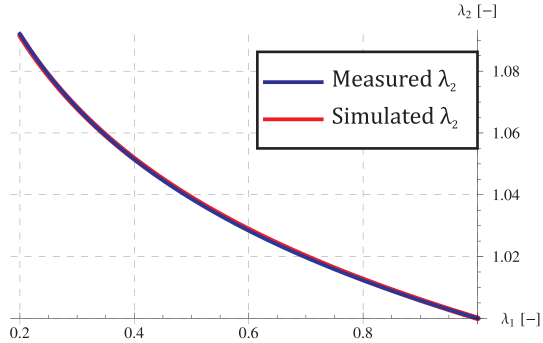

Longitudinal stretch characteristic

Figure 5.4: The results of C-NMD simulations

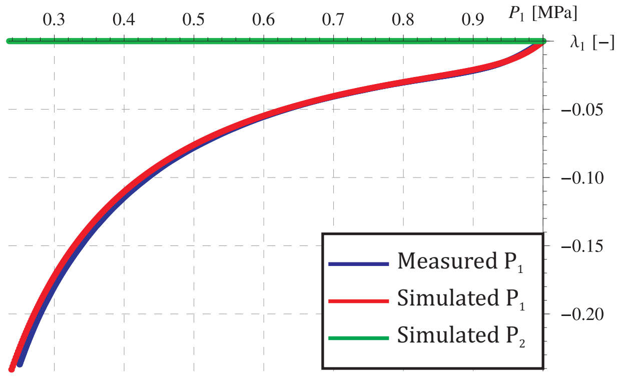

Stress-stretch curves

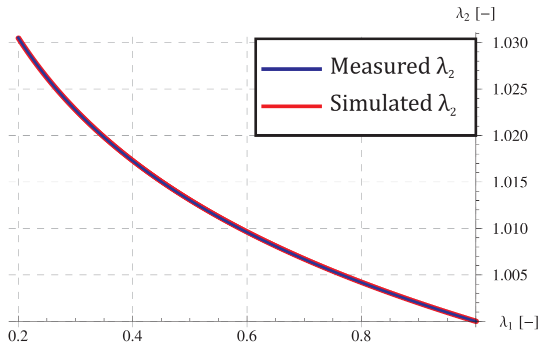

Longitudinal stretch characteristic

Figure 5.5: The results of C-NMD-WL simulations

5.3.3 Compression - Thickness

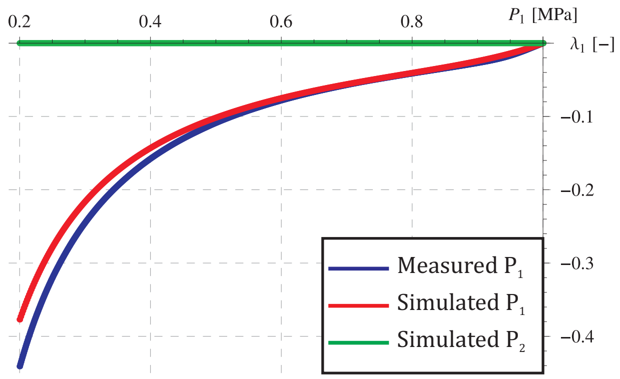

Stress-stretch curves

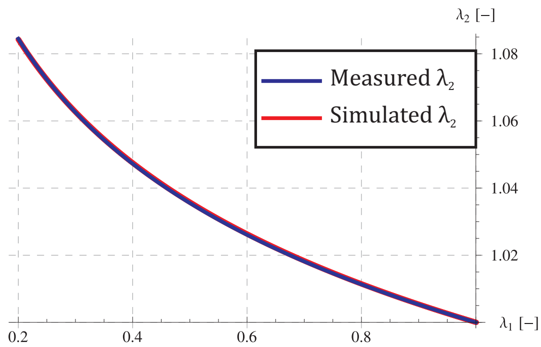

Longitudinal stretch characteristic

Figure 5.6: The results of C-T simulations

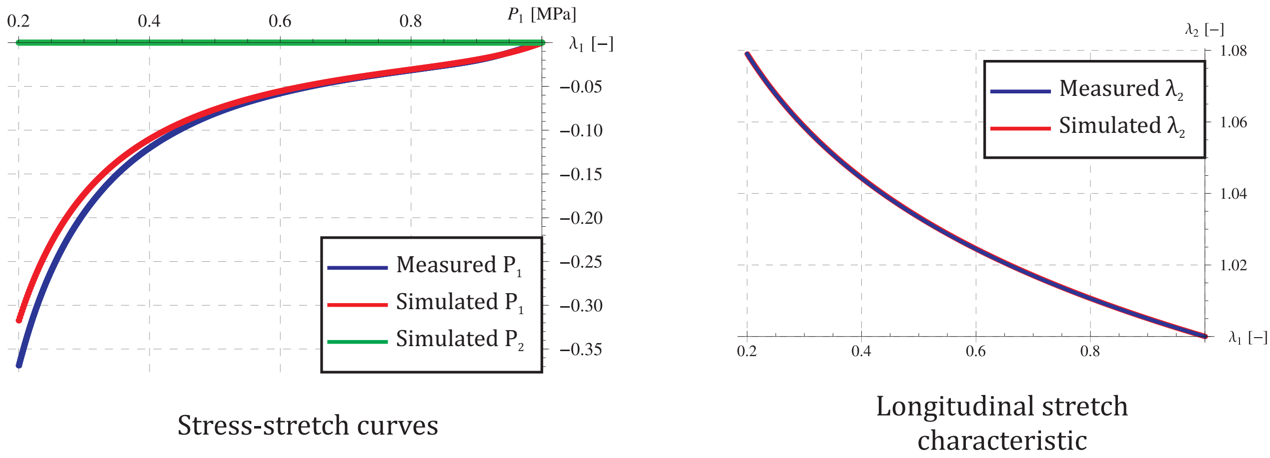

Figure 5.7: The results of C-T-WL simulations

5.3.4 Tension - Machine direction

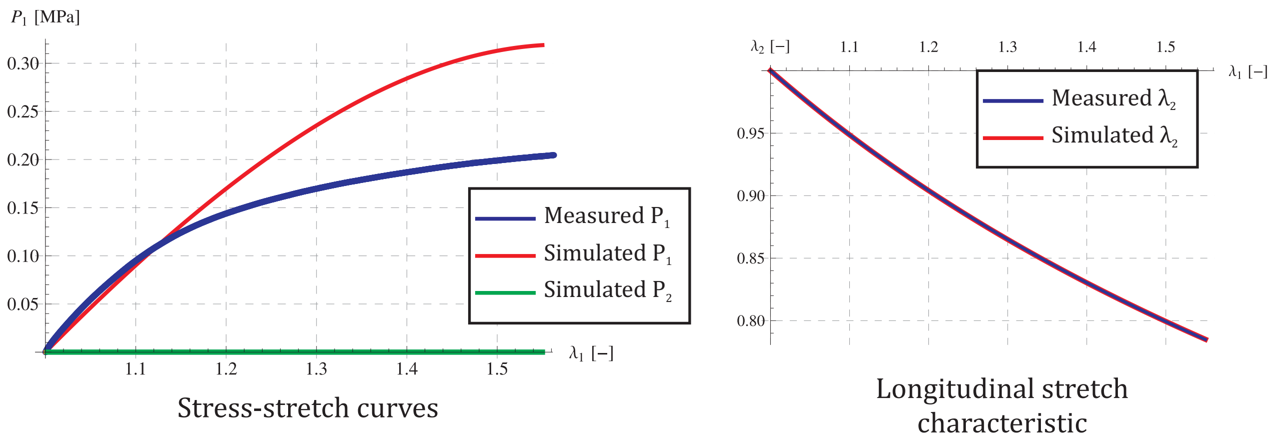

Figure 5.8: The results of T-MD simulations

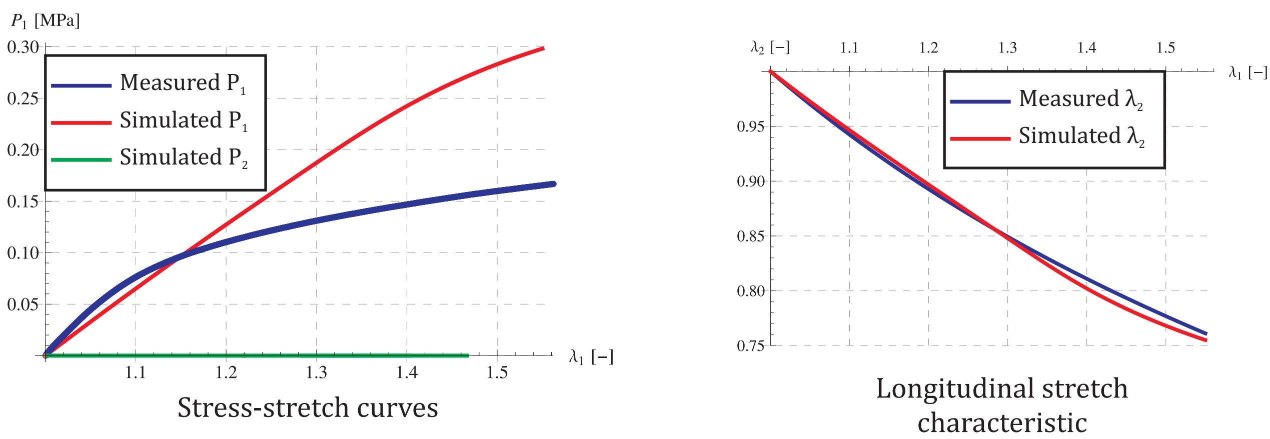

Figure 5.9: The results of T-MD-WL simulations

5.3.5 Tension - Non-machine direction

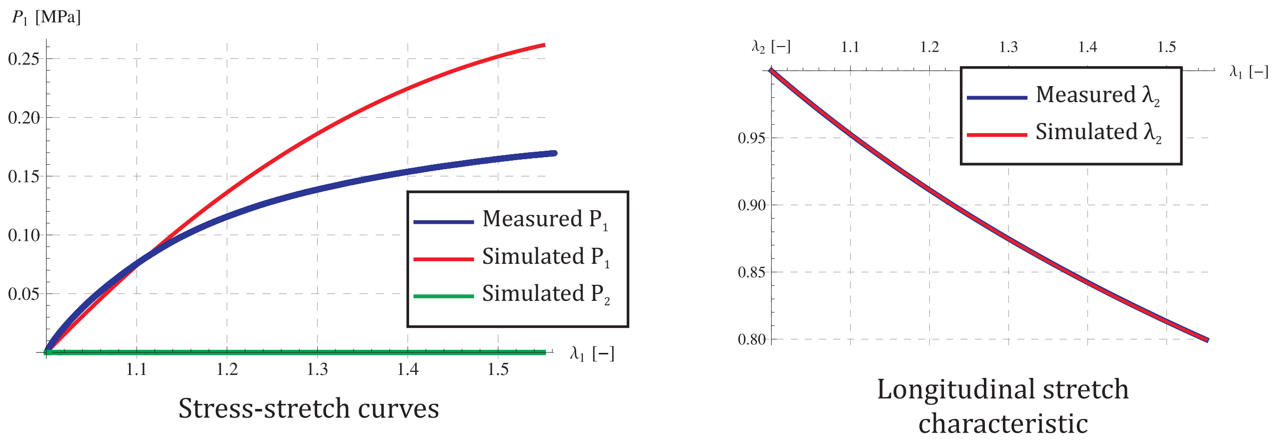

Figure 5.10: The results of T-NMD simulations

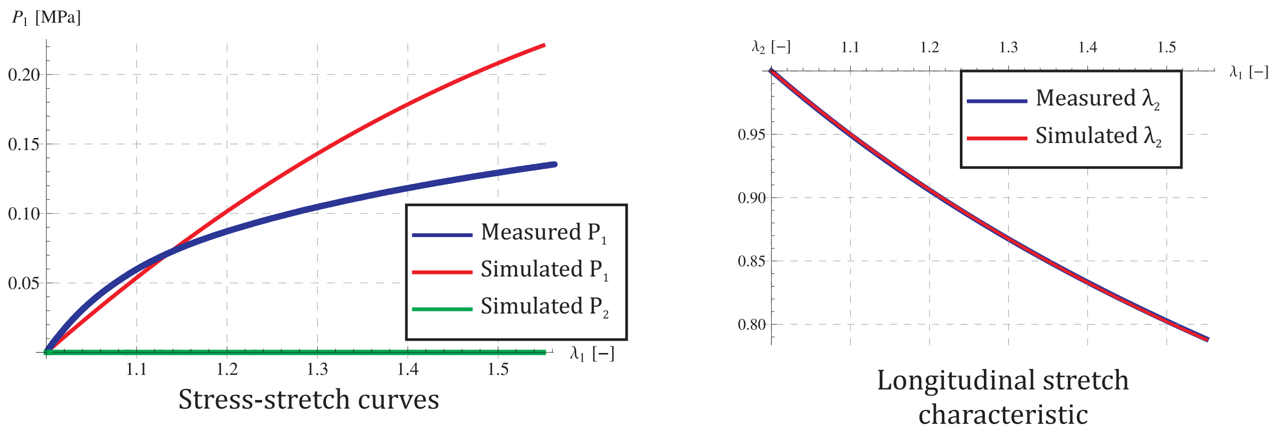

Figure 5.11: The results of T-NMD-WL simulations

5.4 Evaluation of simulation

As the results shows, the numerical simulations differ from the measured results. The errors are determined by using the least square method as

$$e_1 = \sum_{i=1}^{N} (P_{1i} - P_{1i\_Ansys})^2 + P^2_{2i\_fitted} \quad and \quad e_2 = \sum_{i=1}^{N} (\lambda_{2i} - \lambda_{2i\_Ansys})^2, \tag{5.3}$$

where N is the number of measurement points.

Type of specimen	Error (e_1)	Error (e_2)
C-MD	0.3238	$4.96 \cdot 10^{6}$
C-MD-WL	0.1672	$1.41 \cdot 10^{-5}$
C-NMD	0.5385	$3.31 \cdot 10^{-5}$
C-NMD-WL	0.4026	$1.45 \cdot 10^{-7}$
C-T	0.1627	$1.12 \cdot 10^{-5}$
C-T-WL	0.09444	$5.5 \cdot 10^{-7}$
T-MD	8.25245	$3.24 \cdot 10^{-6}$
T-MD-WL	13.5937	0.01698
T-NMD	5.47332	$8.28 \cdot 10^{-6}$
T-NMD-WL	6.50265	$6.11 \cdot 10^{-5}$

Table 5.2: The errors of numerical simulation without layer

In case of compression this difference appears only in the longitudinal stress-stretch ($P_1 - \lambda_1$) characteristic, the error of the cross-direction stretch characteristic is minimal. This is the effect of the following numerical factors. Firstly, as written in *Chapter 4*, because of the error of the model fitting, the material model used in the numerical simulations is just an approximation of the measured data. Besides, the parameters of the material model could be defined as finite length numbers, which can increase the difference between the measured data and the fitted model. Finally, the numerical simulation was executed by using sub-steps so some error occurs by this discrete step simulation. Considering all this factors, the fitted material model approximates well the measured behaviour; the difference appears only in case of large strains ($\lambda_1 < 0.5$).

In case of tension the fitted material model had a bit bigger error, so according to the preliminary expectation the numerical simulation shows bigger differences. The relation of stretches ($\lambda_1 - \lambda_2$) shows only a little error, while in case of stresses the error is bigger. The same error-factors can be observed as in case of the compression. This is mainly caused by the fracturing behaviour of the foam. Firstly, only a few cells fractures, which decreases the area of the cross-section participating in the tension. Although in the post-processing of our measurements this effect was not taken in consideration, thus in case of larger stretches ($\lambda_1 > 1.3$), when the fracture starts, the measured characteristic is damped. Whereas during the finite element simulations, the fracture is not modelled, so the resultant stress-strecth curve do not contain this damping factor, which results in big error.

Nevertheless, the fitted material model approximates the material behaviour well only at smaller stretches ($\lambda_1 < 1.2$), while at bigger stretches the error of the fitted material model is bigger.

As the finite element analysis demonstrates the chosen and fitted Ogden–Storåkers hyperelastic material model is proper for describing the non-linear behaviour of our polyethylene foam.

6
Summary of results

6.1 Summary in English

The skin-layer is a thin layer with modified material parameters on the surface of the polymer foam created during the manufacturing, which results in inhomogeneity. In consequence, this layer affects the overall mechanical behaviour of the foam. The aim of this thesis was to investigate and determine this effect and to set up a suitable material model for the numerical modelling of the foam.

After summarizing the structures and mechanical mechanisms of cellular materials like the polyethylene foam chosen for our investigation, a series of compression and tensile test have been performed. In both cases specimens with and without layer were prepared for all manufacturing directions (MD, NMD, T). With the purpose of creating layer-free specimens I designed a slicer-device to remove the skin-layer adequately. During the measurements, beside the load-displacement values measured by the INSTRON Test System, the cross-directional stretches were video-recorded.

As the result of the post-processing the stress-stretch ($P_1 - \lambda_1$) curves and the relation of the longitudinal and cross-directional stretches ($\lambda_1 - \lambda_{2,3}$) were received. Having analysed the characteristics the effect of skin layer could be determined. The polymer foams strength and elastic modulus increases, thus the foam becomes more fragile which is demonstrated by the decrease of maximum stretch in case of tension. This effect dominates, when the load of direction was machine (MD) or non-machine (NMD), in other words when the load was parallel with the skin layer. In case of thickness direction the degree of the effect was lower.

The mechanical behaviour of the foam was described by using the Ogden–Storåkers hyperelastic material model used especially for compressible foams. Firstly, the stress-stretch function was determined in case of uniaxial load. After, on the basis of the measurement results including the video-processed data, the material parameters of the model were computed using curve fitting methods. The curve fitting required the determination of cross-directional stretch in terms of longitudinal stretch and a correction factor eliminating the error of the measured stretch caused by the geometry of the specimens in case of tension. Finally, a second-order Ogden–Storåkers model was fitted adequately for the characteristics of our polymer foam by minimizing the error, which was bigger in case of tension due to the difference of the tensile characteristics between the model and the measurements.

Finally, all measurements were simulated in ANSYS using the fitted Ogden–Storåkers material model in order to verify the fitted model with the measured data. The results of the simulation shows, that in case of small stretches the fitted model approximates well the measured data. When the stretches are larger the error of the simulation becomes bigger. Although the measured data verifies the numerical calculations, thus the fitted material model is suitable for describing the mechanical behaviour of the polymer foam.

As the result of my thesis the effect of surface skin layer on the overall behaviour of our specific polyethylene foam was determined. Moreover, this behaviour was described by a proper hyperelastic material model used for finite element modelling as well.

6.2 Summary in Hungarian (Az eredmények összefoglalása)

A felületi bőrréteg a gyártás során kialakuló, vékony, megváltozott anyagtulajdonságokkal rendelkező réteg a polimer hab felszínén. A bőrréteg hatására a polimer hab inhomogénné válik, amely befolyásolja a hab eredő anyagi viselkedését, mechanikai tulajdonságait. A dolgozat célja a felületi bőrréteg e hatásának vizsgálata, valamint egy megfelelő anyagmodell felállítása a polimer hab numerikus szimulációja céljából.

Elsőként a polimer habok, mint sejtszerkezetű anyagok, szerkezeti felépítését és mechanikai tulajdonságait összegeztem, melyek alapján nyomó- és szakítóvizsgálatot végeztem egy polietilén habon. A méréseket mindkét esetben bőrréteggel ellátott és bőrréteg nélküli, a gyártási irányoknak (gépirányú, gépirányra merőleges és vastagság irányú) megfelelő próbatesteken végeztem. A bőrréteg nélküli próbatestek létrehozásához egy vágóeszközt terveztem, hogy a felületi bőrréteget megfelelő módon lehessen eltávolítani. A mérések során az INSTRON mérőrendszer által mért erő-elmozdulás értékek mellett a keresztirányú nyúlásokat is rögzítve lettek videokamera segítségével.

A mechanikai vizsgálatok eredményeként az egyes irányokhoz tartozó feszültség-megnyúlás ($P_1-\lambda_1$) valamint keresztirányú nyúlás karakterisztikákat ($\lambda_1-\lambda_{2,3}$) határoztam meg. A bőrréteggel rendelkező és bőrréteg nélküli jelleggörbék összevetéséből a bőrréteg keresett hatása megállapítható: az anyag szilárdsága, rugalmassági modulusa növekszik, így az anyag ridegebbé válik, a maximális megnyúlása szakítómérés esetén lecsökken. Ezek a hatások a legnagyobb mértékben akkor jelentkeznek, amikor a terhelés párhuzamos a bőrréteggel, azaz gépirányban (MD) és arra merőlegesen (NMD), vastagság irányban a hatás mértéke kisebb.

A vizsgált polimer hab mechanikai viselkedését az Ogden–Storåkers hiperelasztikus, speciálisan összenyomható habok leírására létrehozott anyagmodell segítségével írtam le. Az egytengelyű terhelés esetén érvényes feszültség-megnyúlás összefüggés meghatározása után, a modellben szereplő ismeretlen paramétereket a méréssel megállapított karakterisztikára való görbeillesztéssel határoztam meg. A modellillesztéshez szükség volt a fő- és keresztirányú megnyúlások kapcsolatát leíró összefüggés felírására, valamint egy korrekciós tényező meghatározására, amely a próbatest geometriájából származó nyúlásmérési hibát korrigálja szakítómérés esetén. Végül, a hab mechanikai viselkedését egy másodrendű Ogden–Storåkers modellel lehetett megfelelő módon, a hiba minimalizálásával meghatározni. A hiba a szakítómérés esetén adódott nagyobbra, a modellben definiált és a méréssel felvett szakítógörbék közötti eltérés miatt.

Végül, az elvégzett méréseket ANSYS-ban végeselemes analízis segítségével numerikusan is vizsgáltam, annak érdekében, hogy a mért adatokkal összevetve verifikálni lehessen a felállított anyagmodellt. Az eredményekből látható, hogy kisebb megnyúlások esetén a numerikus szimuláció nagy pontossággal közelíti a mért eredményeket, viszont nagyobb nyúlások esetén megnő a szimuláció hibája. Ennek ellenére a mért adatok igazolják a felállított anyagmodell helyességét, így a modell alkalmas a polimer hab anyagi viselkedésének leírására.

Összességében, a dolgozatom eredményeként a felületi bőrréteg eredő anyagi viselkedésre gyakorolt hatását meghatároztam, valamint az anyagi viselkedést egy végeselemes szimulációára is alkalmas hiperelasztikus anyagmodell segítségével leírtam.

Bibliography

[1] Ansys Mechanical 13.0. *Theory Reference: 4.7 Hyperelasticity.*

[2] Inc. ANSYS. Ansys mechanical: Version 13.5.

[3] Allan F. Bower. *Applied mechanics of solids.* CRC Press, 2010.

[4] EA. de Souza Neto, D. Peric, and DRJ. Owen. *Computational methods for plasticity: theory and application.* John Wiley & Sons Ltd., 2008.

[5] Issam Dorghi. *Mechanics of Deformable Solids.* Springer, 2000.

[6] W. H. El-Ratal and P. K. Mallick. Elastic response of flexible polyurethane foams in uniaxial tension. *Journal of Engineering Materials and Technology*, 1996.

[7] International Organization for Standardization (ISO) EN ISO 3386-1. Polymeric materials, cellular flexible - determination of stres-strain characteristic in compression - part 1: Low-density meaterials, 1986.

[8] American Society for Testing and Materials (ASTM) D 3574-03. Standard test method for flexible cellular materials - slab, bonded, and molded urethane foams, 2003.

[9] American Society for Testing and Materials (ASTM) D 3576-98. Standard test method for cell size of rigid cellular plastics, 1999.

[10] Lorna J. Gibson and Michael F. Ashby. *Cellular solids: structure and properties.* Cambridge Univerity Press, 1997.

[11] Storåkers Bertil. On material representation and constitutive branching in finite compressible elasticity. *Journal of the Mechanics and Physics of Solids*, 1986.

[12] Avery Lee. Virtualdub: Edition 1.10.4.

[13] The MathWorks. Matlab edition: 7.14.

[14] Microsoft. Microsoft office 2010: Excel.

[15] Nigel Mills. *Polymer foams handbook.* B&H, 2006.

[16] Jeremiah G. Murphy and Graham A. Rogerson. A method to model simple tension experiments using finite elasticity theory with an application to some polyurethane foams. *International Journal of Engineering Science*, 2002.

[17] Wolfram Research. Findfit function.

[18] Wolfram Research. Mathematica: Edition 7.

[19] Wolfram Research. Nminimize function.

[20] Paul Stevenson. *Foam engineering*. John Wiley & Sons Ltd., 2013.

[21] Adobe Systems. After effects version: Cs5.

Appendix

A.1. Notebook of compression test evaluation

```
date1=Date[];
H0=24;
area={1396.2,1423.5,1501.5,1482};

CSV = {Import["D:\\Users\\test\\C_MD\\Specimen_RawData_1.csv"],
   Import["D:\\Users\\test\\C_MD\\Specimen_RawData_2.csv"],
   Import["D:\\Users\\test\\C_MD\\Specimen_RawData_3.csv"],
   Import["D:\\Users\\test\\C_MD\\Specimen_RawData_4.csv"]};

n=First[Dimensions[CSV]];
CSVDATA=Table[Drop[CSV[[i]],8],{i,1,n}];
FL0=Table[CSVDATA[[i]][[All,2;;3]],{i,1,n}];

Fzero=0.05;
FL=Table[Select[FL0[[i]],#[[2]]>Fzero&],{i,1,n}];
LF=Table[Table[{FL[[j]][[i,2]],FL[[j]][[i,1]]},{i,1,Dimensions[FL[[j]]][[1]]}],
     {j,1,n}];
LF=Table[DeleteDuplicates[LF[[i]],Abs[#1[[1]]-#2[[1]]]<0.001&],{i,1,n}];
F0=0.5;

S0=Table[Interpolation[LF[[i]],InterpolationOrder→1][F0],{i,1,n}]
posH=Table[Position[FL[[i]][[All,2]],Table[Select[FL[[i]][[All,2]],#>F0&][[1]],
     {i,1,n}][[i]]][[1,1]],{i,1,n}]
FLD=Table[Drop[FL[[i]],posH[[i]]-1],{i,1,n}];

FLOK=Table[Table[{FLD[[k]][[i,1]]-S0[[k]],FLD[[k]][[i,2]]},
     {i,1,Dimensions[FLD[[k]]][[1]]}],{k,1,n}];
TL=Table[CSVDATA[[i]][[All,1;;2]] ,{i,1,n}];
SPEED=Table[Table[(TL[[k]][[i,2]]-TL[[k]][[i-1,2]])/(TL[[k]][[i,1]]-TL[[k]]
     [[i-1,1]]),{i,2,Dimensions[TL[[k]]][[1]]}],{k,1,n}];

spmmsec=Table[Mean[SPEED[[i]]],{i,1,n}]
spmmmin=Table[60*Mean[SPEED[[i]]],{i,1,n}]
height=Table[H0-S0[[i]],{i,1,n}]
XLS=FLOK;
dimxls=Table[First[Dimensions[XLS[[i]]]],{i,1,n}];

maxpos=Table[Position[Transpose[XLS[[i]]][[2]],Max[Transpose[XLS[[i]]][[2]]]]
     [[1,1]],{i,1,n}];
data=Table[Drop[XLS[[i]],{maxpos[[i]]+1,dimxls[[i]]}],{i,1,n}];
n=First[Dimensions[data]];
dim=Table[First[Dimensions[data[[i]]]],{i,1,n}];
σλ=Table[Table[{1+-data[[j,i,1]]/height[[j]],-
     data[[j,i,2]]/area[[j]]},{i,1,dim[[j]]}],{j,1,n}];

σmin=1.1*Min[Union[Table[Transpose[σλ[[i]]][[2]],{i,1,n}]]];
σmax=0;
λmin=Min[Union[Table[Transpose[σλ[[i]]][[1]],{i,1,n}]]];
λmax=1;
λmax2=1.05;
```

```
λcut=0.15;
σλ=Table[Select[□λ[[i]],#[[1]]>λcut&],{i,1,n}];
sl=Table[DeleteDuplicates[σλ[[i]],Abs[#1[[1]]-#2[[1]]]<0.001&],{i,1,n}];

λinit=0.85;
σinit=Min[Table[Interpolation[sl[[i]]][λinit],{i,1,n}]];
σmin=1.1*Min[Union[Table[Transpose[sl[[i]]][[2]],{i,1,n}]]];
λmin=λcut;
DIM=Table[First[Dimensions[sl[[i]]]],{i,1,n}];

Young=Table[Table[{sl[[j,i+1,1]],(sl[[j,i+2,2]]-sl[[j,i,2]])/(sl[[j,i+2,1]]-
     sl[[j,i,1]])},{i,1,DIM[[j]]-2}],{j,1,n}];
Ymax=Min[Table[Max[Young[[i]][[All,2]]],{i,1,n}]];
Ysel=Table[Select[Young[[i]],#[[1]]>0.85&],{i,1,n}];

mm=Table[Max[Ysel[[i]][[All,2]]],{i,1,n}];
pos=Table[Position[Ysel[[i]][[All,2]],mm[[i]]][[1,1]]+1,{i,1,n}];
     sldrop=Table[Drop[sl[[i]],pos[[i]]],{i,1,n}];
DIMdrop=Table[First[Dimensions[sldrop[[i]]]],{i,1,n}];
Ydrop=Table[Drop[Young[[i]],pos[[i]]-1],{i,1,n}];
Yinit=1.2*Max[Table[Young[[i]][[pos[[i]]-1]][[2]],{i,1,n}]];

Es=Table[Young[[i]][[pos[[i]]-1,2]],{i,1,n}]
σs=Table[sl[[i]][[pos[[i]],2]],{i,1,n}];
λs=Table[sl[[i]][[pos[[i]],1]],{i,1,n}];
σs=1-λs;
Δσs=σs-Abs[σs/Es];

slc=Table[Table[{sldrop[[i]][[k,1]]+Δσs[[i]],sldrop[[i]][[k,2]]},
     {k,1,DIMdrop[[i]]}],{i,1,n}];
slinit=Table[Table[{1-(i (1-slc[[j]][[1,1]]))/(pos[[j]]+1),i/(pos[[j]]+1)
     slc[[j]][[1,2]]},{i,1,pos[[j]]}],{j,1,n}];
slnew=Table[Union[slinit[[j]],slc[[j]]],{j,1,n}];
DIMnew=Table[First[Dimensions[slnew[[i]]]],{i,1,n}];

date2=Date[];
Δdate=date2-date1;
time=Δdate[[6]]+Δdate[[5]]*60+Δdate[[4]]*3600+Δdate[[3]]*3600*24

Export["D:\\Users\\test\\C_MD_01.csv", Table[slnew[[1]]], "CSV"]
Export["D:\\Users\\test\\C_MD_02.csv", Table[slnew[[2]]], "CSV"]
Export["D:\\Users\\test\\C_MD_03.csv", Table[slnew[[3]]], "CSV"]
Export["D:\\Users\\test\\C_MD_04.csv", Table[slnew[[4]]], "CSV"]
```

A.2. Notebook of tensile test evaluation

```
date1=Date[];
L0=90;
area=247;

CSV={Import["D:\\Users\\test\\T_MD\\Specimen_RawData_2.csv"],Import["D:\\Users\\te
   st\\T_MD\\Specimen_RawData_3.csv"],Import["D:\\Users\\test\\T_MD\\Specimen_RawDa
   ta_8.csv"],Import["D:\\Users\\test\\T_MD\\Specimen_RawData_10.csv"]};
n=First[Dimensions[CSV]]

CSVDATA=Table[Drop[CSV[[i]],8],{i,1,n}];
FL0=Table[CSVDATA[[i]][[All,2;;3]],{i,1,n}] ;
Dim=Table[First[Dimensions[FL0[[i]]]],{i,1,n} ]
max=Table[Max[FL0[[i]][[All,2]]], {i,1,n} ]

limit=Table[Position[FL0[[i]][[All,2]],max[[i]]],{i,1,n}]
First[First[limit[[1]]]]
FLjo=Table[Drop[FL0[[i]], First[First[limit[[i]]]]-Dim[[i]]],{i,1,n}];

lambda01=((FLjo[[1]][[All,1]]-FLjo[[1]][[All,1]][[1]])/L0)+1;
lambda02=((FLjo[[2]][[All,1]]-FLjo[[2]][[All,1]][[1]])/L0)+1;
lambda03=((FLjo[[3]][[All,1]]-FLjo[[3]][[All,1]][[1]])/L0)+1;
lambda04=((FLjo[[4]][[All,1]]-FLjo[[4]][[All,1]][[1]])/L0)+1;
szigma01=((FLjo[[1]][[All,2]]-FLjo[[1]][[All,2]][[1]])/area);
szigma02=((FLjo[[2]][[All,2]]-FLjo[[2]][[All,2]][[1]])/area);
szigma03=((FLjo[[3]][[All,2]]-FLjo[[3]][[All,2]][[1]])/area);
szigma04=((FLjo[[4]][[All,2]]-FLjo[[4]][[All,2]][[1]])/area);

ls01=Table[{lambda01[[i]], szigma01[[i]]},  {i, First[First[limit[[1]]]]}];
ls02=Table[{lambda02[[i]], szigma02[[i]]},  {i, First[First[limit[[2]]]]}];
ls03=Table[{lambda03[[i]], szigma03[[i]]},  {i, First[First[limit[[3]]]]}];
ls04=Table[{lambda04[[i]], szigma04[[i]]},  {i, First[First[limit[[4]]]]}];

date2=Date[];
Δdate=date2-date1;
time=Δdate[[6]]+ Δdate[[5]]*60+Δdate[[4]]*3600+Δdate[[3]]*3600*24

Export["D:\\Users\\test\\T_MD_01.csv", ls01, "CSV"];
Export["D:\\Users\\test\\T_MD_02.csv", ls02, "CSV"];
Export["D:\\Users\\test\\T_MD_03.csv", ls03, "CSV"];
Export["D:\\Users\\test\\T_MD_04.csv", ls04, "CSV"];
```

A.3. Notebook of comparing test results

```
MD01=Import["D:\\Users\\test\\C_MD_01.csv"];
MD02=Import["D:\\Users\\test\\C_MD_02.csv"];
MD03=Import["D:\\Users\\test\\C_MD_03.csv"];
MD04=Import["D:\\Users\\test\\C_MD_04.csv"];

MDWL01=Import["D:\\Users\\test\\C_MD_WL_01.csv"];
MDWL02=Import["D:\\Users\\test\\C_MD_WL_02.csv"];
MDWL03=Import["D:\\Users\\test\\C_MD_WL_03.csv"];
MDWL04=Import["D:\\Users\\test\\C_MD_WL_04.csv"];
limit=Min[First[Dimensions[MD01]], First[Dimensions[MD02]],
     First[Dimensions[MD03]], First[Dimensions[MD04]], First[Dimensions[MDWL01]],
     First[Dimensions[MDWL02]], First[Dimensions[MDWL03]],
     First[Dimensions[MDWL04]]]

lambda = Table[1-0.8 i/limit, {i, 0, limit}];

IPMD01=Table [Interpolation[MD01, 1-0.8 i/limit], {i,0, limit}];
MD01JO= Table[{lambda[[i]], IPMD01[[i]]},  {i, limit+1}];

IPMD02=Table [Interpolation[MD02, 1-0.8 i/limit], {i,0, limit}];
MD02JO= Table[{lambda[[i]], IPMD02[[i]]},  {i, limit+1}];

IPMD03=Table [Interpolation[MD03, 1-0.8 i/limit], {i,0, limit}];
MD03JO= Table[{lambda[[i]], IPMD03[[i]]},  {i, limit+1}];

IPMD04=Table [Interpolation[MD04, 1-0.8 i/limit], {i,0, limit}];
MD04JO= Table[{lambda[[i]], IPMD04[[i]]},  {i, limit+1}];

IPMDWL01=Table [Interpolation[MDWL01, 1-0.8 i/limit], {i,0, limit}];
MDWL01JO= Table[{lambda[[i]], IPMDWL01[[i]]},  {i, limit+1}];

IPMDWL02=Table [Interpolation[MDWL02, 1-0.8 i/limit], {i,0, limit}];
MDWL02JO= Table[{lambda[[i]], IPMDWL02[[i]]},  {i, limit+1}];

IPMDWL03=Table [Interpolation[MDWL03, 1-0.8 i/limit], {i,0, limit}];
MDWL03JO= Table[{lambda[[i]], IPMDWL03[[i]]},  {i, limit+1}];

IPMDWL04=Table [Interpolation[MDWL04, 1-0.8 i/limit], {i,0, limit}];

MDWL04JO= Table[{lambda[[i]], IPMDWL04[[i]]},  {i, limit+1}];
 Mean[{IPMD01[[1]],IPMD02[[1]], IPMD03[[1]], IPMD04[[1]]}];

LAYER=Table[{lambda[[i]], Mean[{IPMD01[[i]],IPMD02[[i]], IPMD03[[i]],
     IPMD04[[i]]}]},  {i, limit+1}];
WLAYER=Table[{lambda[[i]], Mean[{IPMDWL01[[i]],IPMDWL02[[i]], IPMDWL03[[i]],
     IPMDWL04[[i]]}]},  {i, limit+1}];

Export["D:\\Users\\test\\C_MD_LAYER.csv", LAYER, "CSV"];
Export["D:\\Users\\test\\C_MD_WITHOUT_LAYER.csv", WLAYER, "CSV"];
```

A.4. Notebook of cross-directional stretch evaluation

```
BE=Import["D:\\Users\\test\\VIDEO\\MD_01.csv"];
BE2=Import["D:\\Users\\test\\C_MD\\Specimen_RawData_1.csv"];

Dimensions[BE];
tmax= (First[Dimensions[BE]]-1)/23.976;
limit=tmax*23.976
height=20.9011;
H0=24;

IP=Table [Interpolation[BE, i/23.976], {i,0, limit}];
Time = Table[i/23.976, {i, 0, limit}];
TL2= Table[{Time[[i]], IP [[i]]},  {i, limit+1}];
l2min= Min[IP];
l2max= Max[IP];

n=First[Dimensions[BE2]];
BE2OK=Table[Drop[BE2,8] ];

TL=Table[BE2OK[[All,1;;2]]];
IP1=Table [Interpolation[TL, i/23.976], {i,0, limit}];
lambda=H0/height-IP1/height;

lmin= Min[lambda];
lmax= Max[lambda];
pos=First[Dimensions[lambda]-Dimensions[lambdajo]];
TLJO= Table[{Time[[i]], lambdajo[[i]]},  {i, limit+1-pos}];
lambda2jo=Drop[IP, pos];

MIN=lambda2jo[[1]]-1
TL2JO= Table[{Time[[i]], lambda2jo[[i]]-MIN},  {i, limit+1-pos}];

"FITTING";
F=l^(-nu);
mo=FindFit[l1l2, F, nu, l]
```

A.5. Notebook of correction factor determination

```
BE=Import["D:\\Users\\test\\VIDEO_MARKER_CROSSHEAD\\T_MD_01.csv"];
Dimensions[BE];
tmax= (First[Dimensions[BE]]-1)/23.976;
limit=tmax*23.976

CH=Table[BE[[i,2]], {i,1, limit+1}];
Marker=Table[BE[[i,3]], {i,1, limit+1}];
CHMARKER= Table[{CH[[i]], Marker [[i]]},  {i, limit+1}];

F2=m l+b;
mo2=FindFit[CHMARKER, F2, {m,b}, l]
```

A.6. Notebook of curve fitting - compression

```
SL=Import[ "D:\\Users\\test\\C_MD_LAYER.csv"];
Nu2=0.096652;
Nu3=0.048984;
Dim=Dimensions[SL][[1]];

F1=(2μ11)/α11 (λ^(α11)-λ^(-α11β11(1-Nu2-Nu3)))
F12=(2μ11)/α11 (λ^(-α11(Nu2+Nu3)/2) -λ^(-α11β11(1-Nu2-Nu3)))

mo1=FindFit[SL,{F1,( α11*μ11>0)&&( β11>-1/3)},{{ α11,1},{μ11,1},
     {β11,1}},λ,Method→NMinimize]
MO1=F1/.mo1;
MO1l2=F12/.mo1;

ERROR=Sum[((F1/.{λ→ SL[[i,1]]})-(SL[[i,2]]))2+(F12/.{λ→ SL[[i,1]]})^2,{i,1,Dim}];
mo2=NMinimize[{ERROR,( α11*μ11>0)&&( β11>-1/3)},{{ α11,-10,10},{μ11,-10,10},
     {β11,-10,10}},Method→{"SimulatedAnnealing","PerturbationScale"→2,
     "SearchPoints"→100}][[2]]
MO2=F1/.mo2;
MO2lamdba=F12/.mo2;

Sum[(((F1/.mo2)/.{ λ→SL[[i,1]]})-(SL[[i,2]]))^2 +(((F12/.mo1)/.{ λ→SL[[i,1]]})-
     (SL[[i,2]]))^2,{i,1,Dim}]
Sum[(((F1/.mo2)/.{ λ→SL[[i,1]]})-(SL[[i,2]]))^2 +(((F12/.mo2)/.{ λ→SL[[i,1]]})-
     (SL[[i,2]]))^2,{i,1,Dim}]

(*SECOND_ORDER*)

F2=(2μ21)/α21 (λ^(α21)-λ^(-α21 β21(1-Nu2-Nu3)))+(2μ22)/α22 (λ^(α22)-λ^(-α22 β22 (1-Nu2-Nu3)));
F22=(2μ21)/α21 (λ^(-α21(Nu2+Nu3)/2)-λ^(-α21β21(1-Nu2-Nu3)))+(2μ22)/α22(λ^(-α22(Nu2+Nu3)/2-λ-α22β22(1-Nu2-Nu3)));

mo21=FindFit[SL,{F2,( α21*μ21+ α22*μ22>0)&&( β21>-1/3) &&(β22>-1/3)},
     {{ α21,1},{μ21,1}, {β21,1}, { α22,1},{μ22,1}, {β22,1}},λ,Method→NMinimize]
MO21=F2/.mo21;
MO21lambda=F22/.mo21;

ERROR=Sum[((F2/.{λ→ SL[[i,1]]})-(SL[[i,2]]))2+(F22/.{λ→ SL[[i,1]]})^2,{i,1,Dim}];
mo22=NMinimize[{ERROR, ,( α21*μ21+ α22*μ22>0)&&( β21>-1/3) &&(β22>-1/3)},
     { α21, μ21, β21, μ22, α22, β22},Method→{"SimulatedAnnealing",
     "PerturbationScale"→2,"SearchPoints"→100}][[2]]

MEGO22=F2/.mo22;
MEGO22lambda=F22/.mo22;

Sum[(((F2/.mo21)/.{ λ→SL[[i,1]]})-(SL[[i,2]]))^2 +(((F22/.mo21)/.{ λ→SL[[i,1]]})-
     (SL[[i,2]]))^2,{i,1,Dim}]
Sum[(((F2/.mo22)/.{ λ→SL[[i,1]]})-(SL[[i,2]]))^2 +(((F22/.mo22)/.{ λ→SL[[i,1]]})-
     (SL[[i,2]]))^2,{i,1,Dim}]
```

A.7. Notebook of curve fitting - tension

```
SL0=Import[ "D:\\Users\\test\\T_MD_LAYER.csv"];
Nu2=0.511525;
Nu3=0.593596;
c=1.06289;
Dim=Dimensions[SL0][[1]];

L=Table[SL0[[i]][[1]],{i,1,Dim}] ;
L1=L[[1]]*c-1
S=Table[SL0[[i]][[2]],{i,1,Dim}] ;
SL=Table[{c*L[[i]]-L1, S[[i]]}, {i,1,Dim}];

F1=(2μ11)/α11 (λ^α11-λ^(-α11β11(1-Nu2-Nu3)))
F12=(2μ11)/α11 (λ^(-α11(Nu2+Nu3)/2) -λ^(-α11β11(1-Nu2-Nu3)))

mo1=FindFit[SL,{F1,( α11*μ11>0)&&( β11>-1/3)},{{ α11,1},{μ11,1},
     {β11,1}},λ,Method→NMinimize]
MO1=F1/.mo1;
MO1l2=F12/.mo1;

ERROR=Sum[((F1/.{λ→ SL[[i,1]]})-(SL[[i,2]]))2+(F12/.{λ→ SL[[i,1]]})^2,{i,1,Dim}];
mo2=NMinimize[{ERROR,( α11*μ11>0)&&( β11>-1/3)},{{ α11,-10,10},{μ11,-10,10},
     {β11,-10,10}},Method→{"SimulatedAnnealing","PerturbationScale"→2,
     "SearchPoints"→100}][[2]]
MO2=F1/.mo2;
MO2lamdba=F12/.mo2;

Sum[(((F1/.mo2)/.{ λ→SL[[i,1]]})-(SL[[i,2]]))^2 +(((F12/.mo1)/.{ λ→SL[[i,1]]})-
     (SL[[i,2]]))^2,{i,1,Dim}]
Sum[(((F1/.mo2)/.{ λ→SL[[i,1]]})-(SL[[i,2]]))^2 +(((F12/.mo2)/.{ λ→SL[[i,1]]})-
     (SL[[i,2]]))^2,{i,1,Dim}]

(*SECOND_ORDER*)

F2=(2μ21)/α21 (λ^α21-λ^(-α21 β21(1-Nu2-Nu3)))+(2μ22)/α22 (λ^α22-λ^(-α22 β22 (1-Nu2-Nu3)));
F22=(2μ21)/α21 (λ^(-α21(Nu2+Nu3)/2)-λ^(-α21β21(1-Nu2-Nu3)))+(2μ22)/α22(λ^(-α22(Nu2+Nu3)/2-λ-α22β22(1-Nu2-Nu3)));

mo21=FindFit[SL,{F2,( α21*μ21+ α22*μ22>0)&&( β21>-1/3) &&(β22>-1/3)},
{{ α21,1},{μ21,1}, {β21,1}, { α22,1},{μ22,1}, {β22,1}},λ,Method→NMinimize]

MO21=F2/.mo21;
MO21lambda=F22/.mo21;

ERROR=Sum[((F2/.{λ→ SL[[i,1]]})-(SL[[i,2]]))2+(F22/.{λ→ SL[[i,1]]})^2,{i,1,Dim}];
mo22=NMinimize[{ERROR, ,( α21*μ21+ α22*μ22>0)&&( β21>-1/3) &&(β22>-1/3)},
     { α21, μ21, β21, μ22, α22, β22},Method→{"SimulatedAnnealing",
     "PerturbationScale"→2,"SearchPoints"→100}][[2]]

MEGO22=F2/.mo22;
MEGO22lambda=F22/.mo22;
Sum[(((F2/.mo21)/.{ λ→SL[[i,1]]})-(SL[[i,2]]))^2 +(((F22/.mo21)/.{ λ→SL[[i,1]]})-
     (SL[[i,2]]))^2,{i,1,Dim}]
Sum[(((F2/.mo22)/.{ λ→SL[[i,1]]})-(SL[[i,2]]))^2 +(((F22/.mo22)/.{ λ→SL[[i,1]]})-
     (SL[[i,2]]))^2,{i,1,Dim}]
```

A.8. Notebook of numerical simulation evaluation

```
MPL=Import[ "D:\\Users\\test\\C_MD_LAYER.csv"];
Nu2=0.096652;
Nu3=0.048984;
λ2=λ^(-(Nu2+Nu3)/2);

BE=Import[ "D:\\Users\\test\\ANSYS\\C_MD.csv"];
BEOK2=Table[Drop[BE,1] ];
BEOK=Insert[BEOK2, {0,0,0,0,0},1];
Dim=Dimensions[BEOK][[1]];
t=Table[BEOK[[All,1]]];
P1=Table[BEOK[[All,3]]];
P2=Table[BEOK[[All,5]]];
l=Table[BEOK[[All,2]]];
l2=Table[BEOK[[All,4]]];
APL=Table[{1+l[[i]], P1 [[i]]},  {i, Dim}];
AL1L2=Table[{1+l[[i]], 1+l2 [[i]]},  {i, Dim}];
AL1P2=Table[{1+l[[i]],P2 [[i]]},  {i, Dim}];
DI=Dimensions[APL][[1]]

HIBA1=Sum[((APL[[i,2]]-Interpolation[MPL, APL[[i,1]]])2+
     (AL1P2[[i,2]])^2),{i,1,DI}]
HIBA2=Sum[(AL1L2[[i,2]]- λ2/.{λ→ AL1P2[[i,1]]})2,{i,1,DI}]
```